Groundwater Prospectivity Mapping Using Integrated GIS, Remote Sensing, and Geophysical Techniques; A Case Study From Northeastern Nigeria

Yusuf, A.[1], Lim, H. S.[2*] and Ahmad Abir, I.[3]

1. Ph.D. Student, School of Physics, University Sains Malaysia, Penang, Malaysia
2. Associate Professor, School of Physics, University Sains Malaysia, Penang, Malaysia
3. Assistant Professor, School of Physics, University Sains Malaysia, Penang, Malaysia

Abstract

An integrated GIS, Remote sensing, and Geophysical techniques have been successfully applied to generate the previously non-available groundwater prospectivity map for the present study area. Selected thematic maps were integrated using the weighted sum tool of the spatial analyst tool of the ArcGIS software. The five thematic maps used are: lithology map, drainage density map, slope map, lineaments density map, and the topographic map of the area. The groundwater prospectivity map generated was reclassified into low, moderate, high, and very high potential zones on the basis of their assigned layer rank, which also depends on their degree of influence on groundwater occurrence. Areas around Gombe, Wuyo, Deba, Alkaleri, Kaltungo, Misau, Nafada, Bajoga towns are the regions that showed very high prospects for groundwater occurrence. Data processing filters such as: horizontal derivatives, Analytic signal processing, 3D-Euler depth estimation was applied on the magnetic data in order to map structures and lithologic contacts before its subsequent integration with other structural lineaments as a thematic layer. Vertical Electrical Sounding (VES) data were used to compute hydraulic conductivity, and Transmisivity etc. for the acquiferous layers identified. The results of the present study showed some regions that are classified as highly prospective to be consistent with high transmisivity and high yield values. The final outcome (groundwater potential map) of this research demonstrated that GIS/remote sensing, and the geophysical technique employed is a very powerful tool for generating groundwater prospectivity map, which is very vital in terms of planning for groundwater exploration and exploitation.

Keywords: Multiple criteria, Analytic Hierarchy process, Groundwater, Geographic Information System, Thematic maps.

1. Introduction

The introduction of geospatial techniques (GIS and remote sensing) and other air-borne geophysical means of investigation for structures and other features of hydrogeological importance have contributed immensely towards simplifying procedures of structural mapping (Epeju et al., 2017), and the subsequent understanding of groundwater potentials of different regions of the globe as revealed by the works of Pradhan (2009), Hammouri et al. (2012), Nampak et al. (2014), and Razandi et al. (2015). The methods have actually been found to be cost-effective and shorten the time to be spent on field mapping of structures. It also enables the structures that are located in practically accessible areas to be mapped easily. Lineaments are usually found to be in form of joints, faults, sills, dykes, foliations, bedding planes etc. (Mogaji et al., 2011).

Lineament's pattern, density, intersections, and the intersections - density of the lineaments of a rock outcrop in a given area are found to be very significant in terms of revealing high potential areas for groundwater occurrence (Tahir et al., 2015; Epeju et al., 2017). Moreover, siting of boreholes along or away from areas of high lineaments density as well as high lineaments intersection density are found to affect boreholes yields either positively or negatively (Hammouri et al., 2012; Chuma et al., 2013; Senthil Khumar and Shankar, 2014).

Water as an adage said is equal to life; therefore, increased population in our local communities is synonymous with increased demand for water supply. Water is a very significant resource that supports the existence of humans and other living things on the earth (Yusuf et al., 2018). Its

---

*Corresponding author: hslim@usm.my

inadequacy results to numerous health and social problems (Elbaz, 2008). There are two main categories of water resources, surface water resources, and ground water resources. The surface water resources such as rivers, streams, oceans, and lakes are not only seasonal in nature, but mostly found to be polluted and as such not suitable for domestic utilization. Whereas, groundwater resources are more reliable, widespread in occurrence and less likely to be polluted compared to the surface water resources (Talabi and Tijani, 2011; Ahmed II et al., 2013).

Furthermore, not all communities in the research area are connected to the municipal water supply schemes; but the populace usually resorts back to unhealthy surface water to meet their daily water consumption needs. Therefore, to checkmate the increase demand for water needs because of an increase in population in our communities, there will be a need for elaborate well-planned groundwater exploration studies using surface and sub-surface structural mapping, remote sensing data integration through the use of GIS techniques, since surface waters are intermittent.

Generally speaking, several countries of the world have prepared their groundwater maps that help in providing guidance to governments, and other stakeholders in the areas of evaluation, planning and managements of water resources in their domains (Elbeich, 2014). However, the above-mentioned very important map (information) is obviously not available in Nigeria. This is attributed to the neglects of the use of the faster, cost-effective, GIS, remote sensing, and airborne geophysics in the study of groundwater resources of various regions of the country (Ahmed II and Mansour, 2018). An assessment of the few GIS and remote sensing studies in groundwater resources distribution in Nigeria by Ahmed II and Mansour (2018) shows that Southwestern part of Nigeria as the most explored region in terms of the use of GIS and remote sensing in groundwater studies, followed by the North central, Northwest/ South, Southeast, and Northeast (in descending order of published work) with the zero record of any research work in this regard. Hence the need to embark on this kind of research that is the first of its kind in

this region that is aimed at providing the information needed for the better understanding of the groundwater prospectivity of this area.

Inadequate information regarding groundwater resources, especially in Nigeria and other developing nations is one of the major hurdles toward achieving sustainable water resources developments (Ahmed II and Mansour, 2018). This problem continued to affect the evaluation, planning, and economic growth of these countries.

The present research work was carried out because of the consideration of the way and manner in which the inhabitants of this region continued to battle with the problem of inadequate, non-qualitative and portable water supply attributable to poor understanding of the hydrogeological structural features of the area (Olasehinde, 1999; Fashae et al., 2014), complex nature of the geology and the tectonic set up of the area and the drilling of boreholes with poor yields (Offodile, 2014). Therefore, in order to bridge this knowledge vacuum (gap) existing with regards to poor understanding of structures of hydrogeological importance around this area, as well as the non-availability of groundwater potential map for the study area, which will go a long way in reducing the groundwater exploration challenges of this region, this research was undertaken.

It is a generally accepted idea that the distribution of groundwater within the earth's sub-surface is strongly influenced by porosity and permeability of the rocks, geomorphology, slopeness of an area, drainage density pattern, as well as the distributions of secondary porosity features that includes both surface and near surface structures (lineaments) such as faults, joints, beddings planes (El-Naqa et al., 2009; Mogaji et al., 2011) etc. Hence, the use of airborne magnetic data to map relatively deep seated magnetic lineaments, magnetic lineaments densities, and the subsequent use of Landsat-08, and Shuttle Radar Topographic Mission - Digital Elevation Model (SRTM-DEM) data for surface lineaments mapping, surface lineaments density computation, as well as their intersection densities, drainage density, lithology, topography and slope pattern of the

research area in order to integrate them using GIS method for multi-criteria evaluation (**MCE**) technique (Sikdar et al., 2004; Sultan et al., 2008; Mohammed-Aslam et al., 2010). A groundwater prospectivity map of the study area was finally produced after integrating both the geophysical and remote-sensing data using GIS technique.

2. Location, Geology and Hydrogeology of the Study area:

The present study area is located in the Gongola sub-basin of northeastern Nigeria, and the adjoining basement complex (Figure 1) covering about 49,284 km^2. It is defined by the following coordinates: Longitudes; 10^000'E to 12^000'E, and latitudes; 9^030'N, to 11^030'N. Major towns within the study area include Gombe, Dukku, Darazo, Nafada, Kaltungo, Tula, Giade, Alkaleri, Wuyo, Misau, Dadiya, Lamurde, and Deba (Figure 2).

The study area is characterized by low, very low, and high altitudes (highly elevated) zones. Areas towards the western and eastern parts of the study area show high elevation compared to the central and northern parts, which has low to very low topography (Figure 3). Coincidentally, the areas

depicting higher elevation within the study area are occupied by the exposures of Precambrian basement rocks, especially in the western parts, and the exposures of the same basement outcrops as well as that of older basaltic plugs outcropping towards the eastern parts of the area (NGSA, 2009, Figure 2). Some of the low to very low elevated regions are characterized by the distributions/exposures of cretaceous to recent sediments and thus formed the Gongola basin outlines. These areas are characterized by a lot of streams channels that help in revealing the sedimentary succession within the basin, which include the Aptian – Albian Bima Formation found to be lying unconformably on the Precambrian basement followed by the deposition of transitional Yolde Formation; the Yolde formation is further overlain by the fully marine Pindiga Formation characterized by a lot of limestone and shales composition. The Pindiga formation is again over lain by the fluvial (Maastrichtian) Gombe Formation. The Gombe Formation consists of lithologies like sandstones, siltstones, and mudstones (Abubakar, 2006; Zaborski et al., 1997; Obaje, 2009; Tukur, 2015).
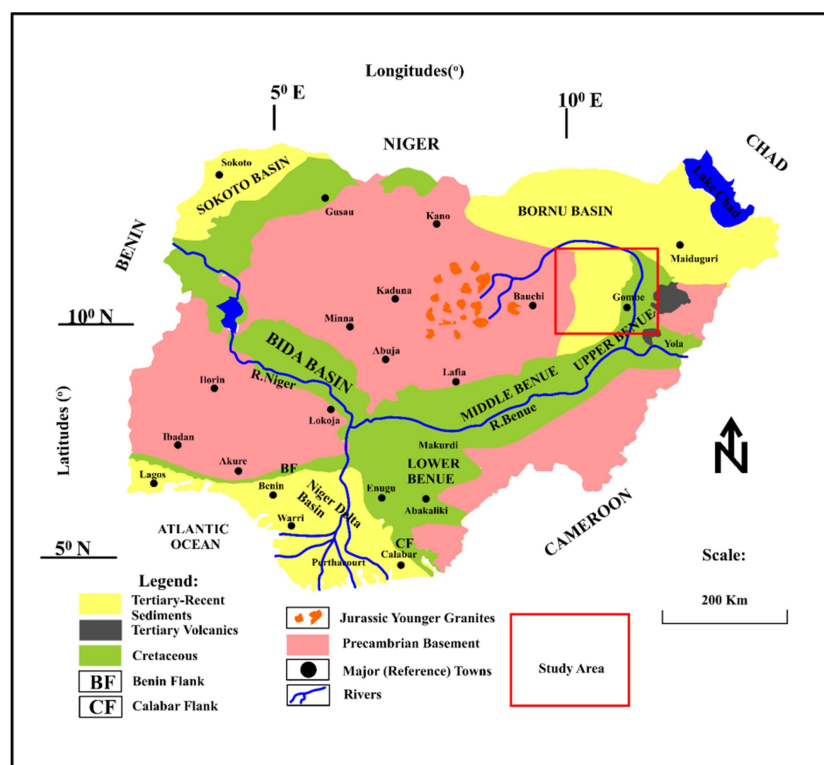

Figure 1. Geological map of Nigeria displaying the location of the study area with a red colored hollowed Square (modified from Obaje, 2009).
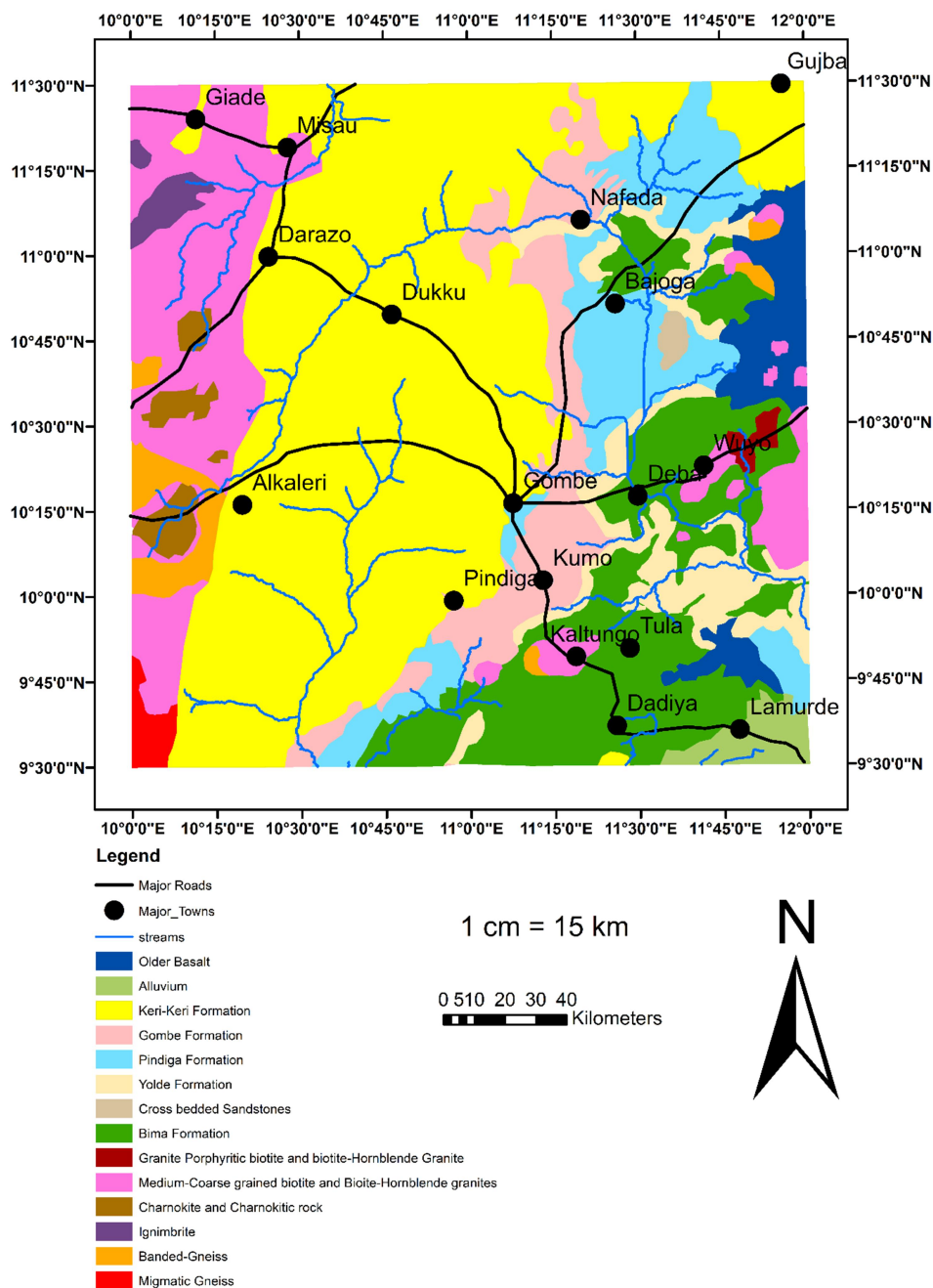
Figure 2. An enlarged view of the Geological map of the study area (Modified after, NGSA, 2009).

The youngest lithological units overlying the Gombe Formation unconformably is the palaeogene Kerri-Kerri Formation, which is composed of clays, and laterites outcropping at the extreme western parts of the Gongola sub-basin's border with the crystalline basement rocks (Figure 2) (Abubakar, 2006). The crystalline basement rocks outcropping at the extreme western parts of the study area comprises of medium to coarse grained biotie-biotite hornblende granites, banded gneiss, ignimbrites, migmatites gneiss and the pyroxene bearing granites popularly known as charnokytes (Figure 2, above). Similarly, rocks outcropping towards the extreme eastern parts of the study area are; medium – coarse grained biotite – biotite granites, banded gneisses, porphyritic biotite – biotite hornblende granites and the older basaltic plugs known as Biu and Lunguda basalts. Moreover, areas around Gombe and Kaltungo lie on or very close to a basement outcrop usually known as "inlier". This area consists of medium to coarse grained biotite-hornblende granites as well as porphyritic biotites granites with some basalts outcrops

surrounding it (Mboringong et al., 2013).
Hydro-geologically, the study area can be seen to be composed of both basement complex, the basalts plugs and the sedimentary rock distributions. The basement complex terrains are found to be consisting of three (3) to four (4) sub-division hydro-geologically. These sub-divisions include top layer, which is usually found to be top soil/ lateritic soil, then the layer immediately below it is the weathered basement layer, and/or fractured basement units, finally the fresh or impervious and unfractured basements at the bottom. The weathered overburden is underlain by the fractured basements at the bottom. The weathered overburden or the fractured basements are usually found to be water bearing unit in the set-up (Zaborski et al., 1997), while the non-fractured and the non-porous unit at the bottom bears no water at all.

However, in the sedimentary sections of the study area, the distribution of groundwater is a little bit more variable, as it depends on the porosity and permeability of the individual lithological units found in each of the formations found in the study area as follows; Kerri-Kerri Formation (has deep layered aquifer), Gombe Formations that is classified as Aquifer to Acquicludes, Pindiga Formation as non Acquiferous due to the thick shale and limestone deposits. While, the Yolde and the Bima Formation are considered to be acquiferous due to the possession of high porosity and permeability of its Sandstone units (Lovelyn et al., 2016).

3. Materials and Methods
3-1. Materials
The materials used for the present research work involves new high-resolution aeromagnetic data obtained from Nigerian Geological Survey agency. This data was acquired by the Fugro-Air Services Limited between the years of 2004 and 2009. This data is the latest data acquired with a higher resolution so far, it was acquired with a flight line separation of 500 m, 80 m flight height, and a 2 km Tie-line intervals along NE-SW pattern (orientation).

Other materials used in the research include shuttle radar topographic digital elevation model (SRTM-DEM) as well as the LANDSAT-08 data, that was downloaded freely from www.earthexplorer.usgs.gov in small parts (sheets) that were later merged to form a separate composite DEM, and Landsat-08 data of the study area. A number of software such as ArcGIS, Oasis-Montaj, ENVI, Rock Works, and Global Mapper were used in the processing of these data.

3-2. Methods
3-2-1. Lineaments mapping from DEM data
As mentioned above, the SRTM-DEM and the Land Sat-08 data were obtained from the United States Geological Survey Agency website (www.earthexplorer.usgs.gov). The data were downloaded in different sheets with 30 m resolution and were merged into a single bigger (composite) unit (Figure 8-a) using the "Mosaic Raster" tool of the ArcGIS environment. "Contours and drainage extraction" were performed on the composite DEM raster using the "spatial analyst tools" of the ArcGIS software. Hence, a topographic (location) map of the study area was generated (Figure 3). The composite DEM raster was imported into Global Mapper for Lineament mapping. The lineaments were then mapped manually from the DEM raster. The manual means of mapping was adopted in order to avoid the mapping of artificial (man-made) features that are not of interest to the present research, especially when an automatic means of lineaments extraction is used (Meijerink, 2007). The mapped lineaments were extracted on the basis of variation in tone, texture, and some geomorphological outlook of the images. The mapped lineaments were then imported in to the ArcGIS software for the generation of the lineaments distribution contour maps (Figure 8-a to 8-d). Other parameters like the lineaments intersection, lineaments density, and lineaments intersection density were also generated using kernel density algorithm (Silverman, 1986) in the ArcGIS environments. Moreover, the distribution of the lineaments was plotted in an azimuth-rose plot using "Rock work" software (Figure 8-e).
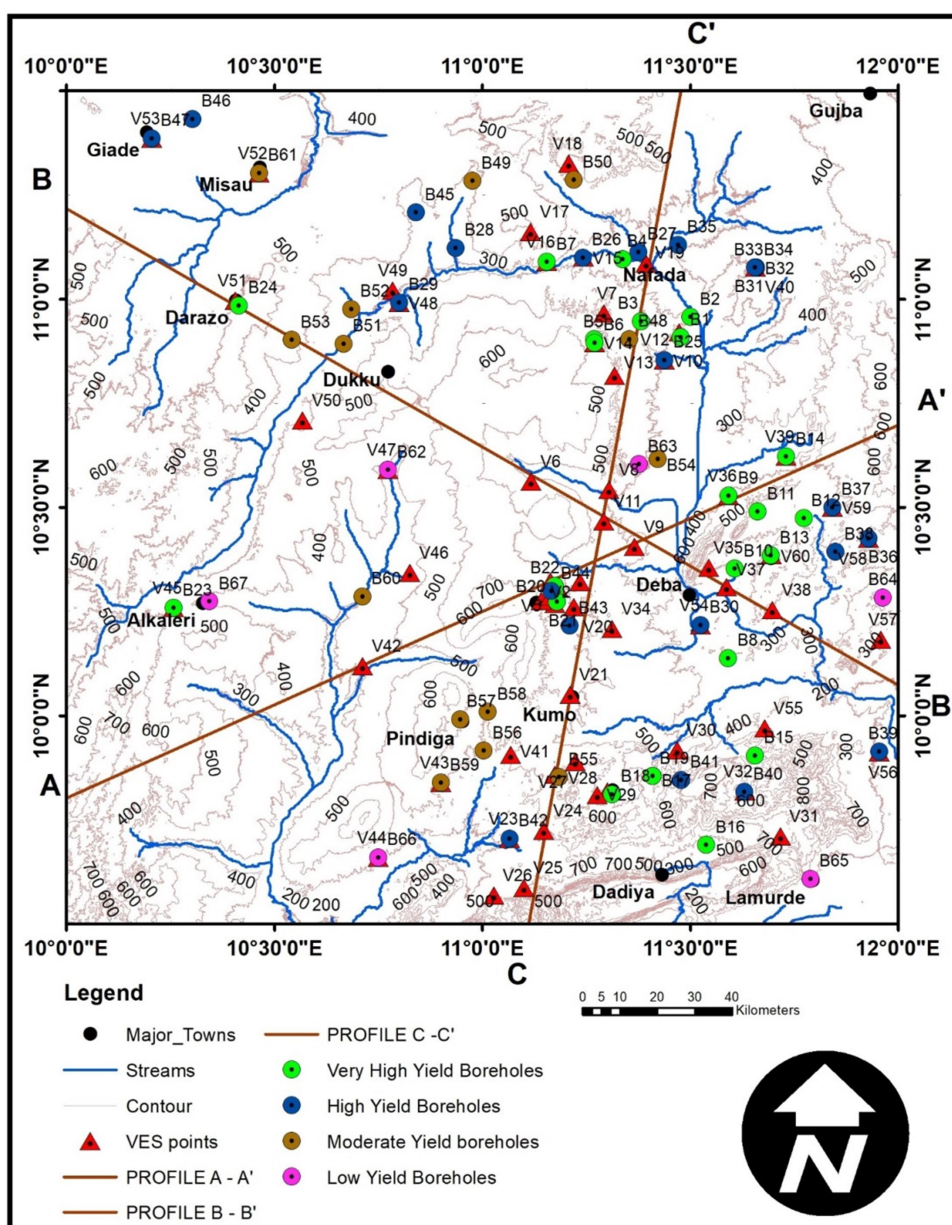
Figure 3. The topographic map showing spatial distributions of VES points, boreholes distributions and the geomorphologic features of the study area.

3-2-3. Lineaments mapping from Landsat-08 data

The Lansdsat-08 data was downloaded from the same source with the DEM data used for this study. The downloaded data being in small sheets of 30 m resolution like the Dem data, it was exported to ENVI software for merging into a single unit that constitutes the size of the study area. Band 5, 6, 8 and 9 were extracted and merged to form the composite land-sat image used for the lineament extraction. The merged image was imported into Global mapper, and finally to ArcGIS for lineament extraction and processing. Similar criteria and treatment given to the DEM data (mentioned above) while performing the lineament mapping was also applied to the Landsat-08 image imported. Hence, the Landsat-derived lineament distribution map (Figure 9-a), lineament-density map (Figure 9-b), lineament-intersection map (Figure 9-c), and lineament-intersection-density maps (Figure 9-d) were generated employing the same kernel density approach using the ArcGIS software. The rose diagram (Figure 9-e) of the Landsat lineaments was produced using the rock work software.

3-2-4. Lineaments mapping from Aeromagnetic data

On the aspect of aeromagnetic data used for this research, the data was also acquired in form of smaller grids (30' by 30') that were later merged to form a bigger composite grid, which serves as the total magnetic intensity (TMI) grid for the study area (Figure 4-a). This was done using multiple grids knitting process of the Geosoft-oasis montaj software. The (TMI) map (Figure 4-a) was computed using a 100 m grid interval using the minimum curvature method of gridding. This satisfied one-third to one-fifth of flight line separations requirements suggested by Dentith (2011). Since the present study area is positioned in a low latitude zone, which implies the magnetic anomalies tend to be non-centralized (skewed) over their causative bodies. This can be attributed to the bipolar nature of the earth's magnetic field (Stacey, 1961). Thus, the reduction to equator (RTE) correction was applied to the TMI grid. The RTE offers more reliable outcomes compared to the reduction to pole (RTP) correction in a low latitude areas (Jain, 1988). Hence, the TMI corrected to magnetic equator (RTE-TMI) map (Figure 4-b) was generated. The RTE filter helps in re-aligning the magnetic anomalies on their causative bodies. The RTE correction was performed using an angle of inclination of -1.82° and a declination angle of -0.63°.

The total magnetic field grid was later subjected to regional-residual separation using polynomials fitting process. The polynomials of order 2nd degree were used to generate the residual map (Figure 4-c).

In order to enhance and map the sub-surface linear structural features and lithological contact zones, the magnetic data was further subjected to some filtering techniques that include; horizontal derivative computation, Euler deconvolution computation, and Analytic signal computations.

The residual map was first subjected to horizontal derivatives computations using the Oasis Montaj software using Cordell and Grauch (1985) algorithm as shown below:

$$\frac{\partial T}{\partial H} = \sqrt{\left(\frac{\partial T}{\partial X}\right)^2 + \left(\frac{\partial T}{\partial Y}\right)^2} \qquad (1)$$

where; $\frac{\partial T}{\partial H}$, $\frac{\partial T}{\partial X}$, and $\frac{\partial T}{\partial Y}$ denotes total horizontal magnetic derivatives, derivatives with respect to x-direction, and derivatives with respect to y-direction respectively.

The total horizontal derivative filter applied helped in revealing linear features from the magnetic data processed (Figure 4-a). The horizontal derivative image map was also used to map the linear features based on the variation in tone, texture, and some geomorphological outlook of the images just like in the case of the DEM, and the Landsat 08 images. The same process of using kernel density algorithm in the ArcGIS environment was used to generate magnetic-derived lineament "lineament density map (Figure 10-b), lineament intersection map (Figure 10-c) and the lineament intersection density map (Figure 10-d)". The rose diagram (Figure 10e) of the magnetic lineaments was produced using the Rock Work software.

3-2-5. Analytic Signal (AS) and Euler depth (EUD) maps computation

According to Nabighian (1984) and Roest et al. (1992), the analytic signal of a given magnetic data can be obtained by calculating the square root of the total squares of a given magnetic signature differentiated along the x, y, and z directions of the magnetic field as expressed below:

$$\frac{\partial T}{\partial A} = \sqrt{\left(\frac{\partial T}{\partial X}\right)^2 + \left(\frac{\partial T}{\partial Y}\right)^2 + \left(\frac{\partial T}{\partial Z}\right)} \qquad (2)$$

The analytic signal filter was basically applied directly on the total magnetic intensity (TMI) field map of the study area, as this filter is insusceptible to IGRF field direction, which implies that it does not need to be preceded by reduction to equator correction. This filter helps in mapping contacts of major lithological units found in the study area. viz; Basement, Sedimentary, and Volcanic rocks (Figure 5).
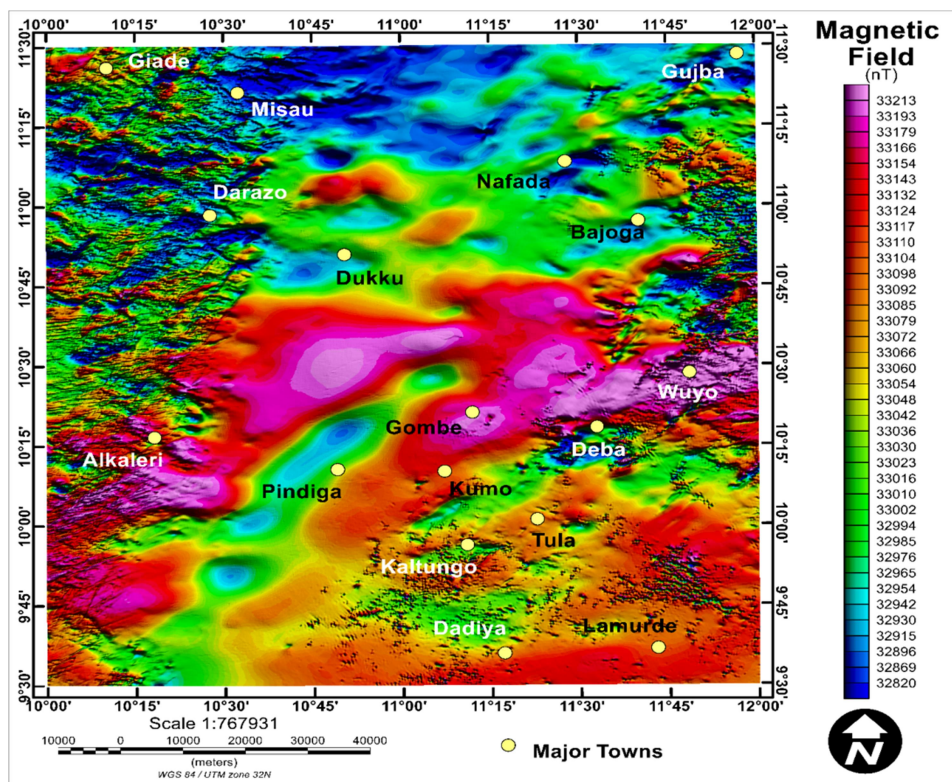
(a)
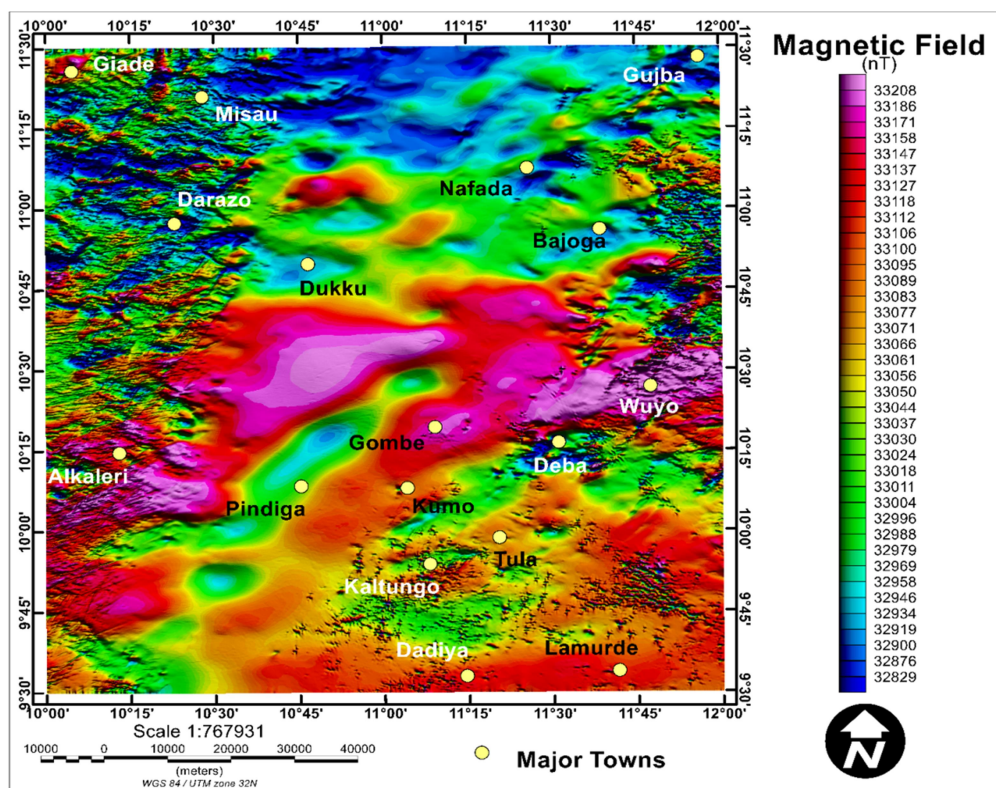
(b)
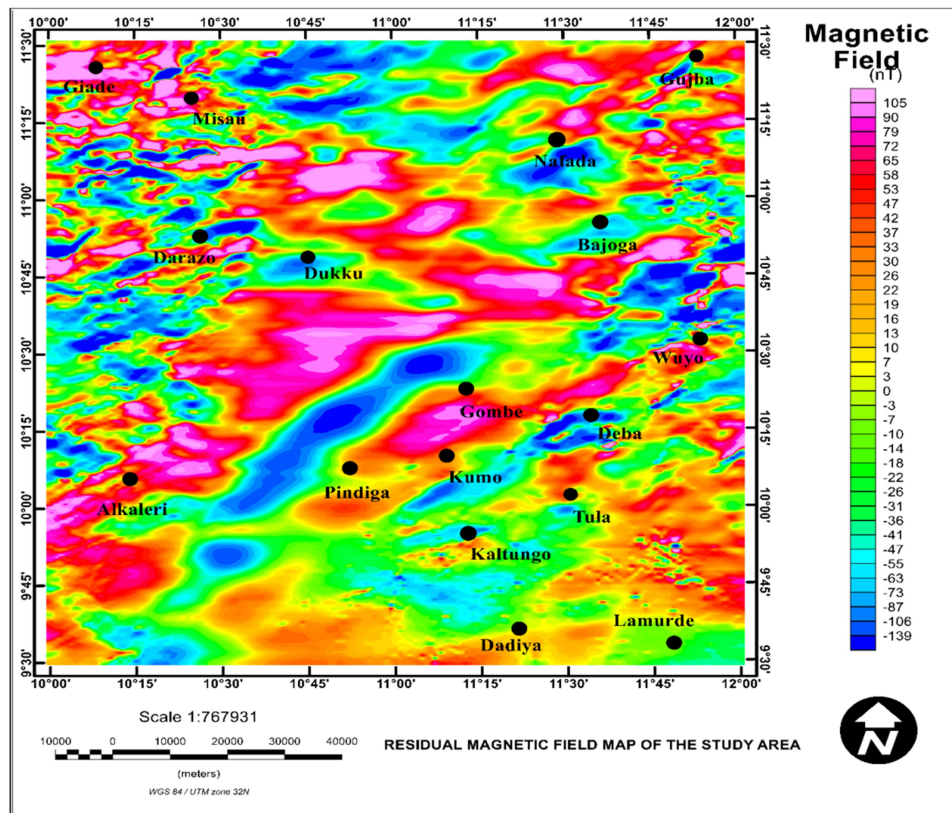
(c)

Figure 4. a) Total magnetic field intensity (TMI) map of the study area, b) Reduced to magnetic equator (RTE-TMI) map of the study area, c) Residual magnetic field map of the study area generated through polynomials fitting process.
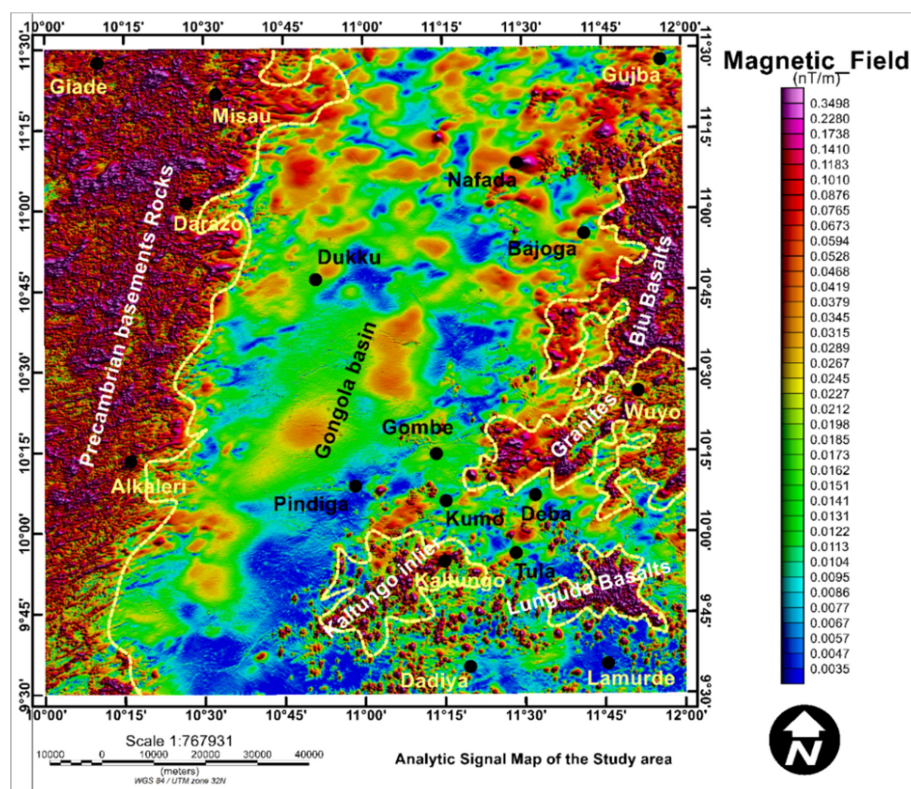
Figure 5. Analytic signal map showing the major rocks distribution as revealed by their magnetic contrasts.

In an attempt to further map the depth to subsurface structural lineament found within the study area. A 3D Euler depth deconvolution estimation method was applied to the RTE-TMI map of the research area. It was performed by employing the standard 3d Euler method, which is based solely on the homogeneity equation that provided a relationship between the magnetic field data and its related gradients constituents as shown below:

$$N(B - T) = (x - x_0)$$
$$\frac{dT}{dx} + (y + y_0)\frac{dT}{dx} + (z - z_0)\frac{dy}{dx} \qquad (3)$$

where, $\frac{\partial T}{\partial H}$, $\frac{\partial T}{\partial X}$, and $\frac{\partial T}{\partial Y}$ are the field derivatives in the x, y, and z directions, N stands for degree of homogeneity or structural index, B is total regional magnetic field value and x_0, y_0, and z_0 stand for the position of the causative sources, while T stands for the total magnetic field at (x, y, and z.).

The Euler depth estimation method locates its source using a given structural index. The current study employed the use of these parameters in the computation of the Euler depth map for this area (Figure 6). These include Window size of 7 km, Structural

index: 1 (for faults and fractures delineation), maximum acceptable distance: 7.5 km, and a maximum % depth tolerance of 15%.

3-2-6. Integrated (Composite) Lineament Map Production

Each of the individual lineament distribution image (maps) of the DEM, Landsat-08, and the Magnetic data was first subjected to the generation of their Euclidean distances using the spatial analyst tool of the ArcGIS software. The different Euclidean distance image maps for each of the three different data types were re-classified between 0, and 100, with 0, being an area that is devoid of lineaments, while 100, stands as the area of occurrence of lineaments. The reclassified Euclidean distance images of the three data types generated were then integrated together by applying the "Math Algebra" tool found within the Spatial "Analysts tool" of the ArcGIS software. The integrated image generated, which shows the lineament coincidence image was finally used to map the integrated lineaments for the study area (Figure 11-a). The rose diagram (Figure 11-d) of the integrated lineaments was produced using the rock work software.
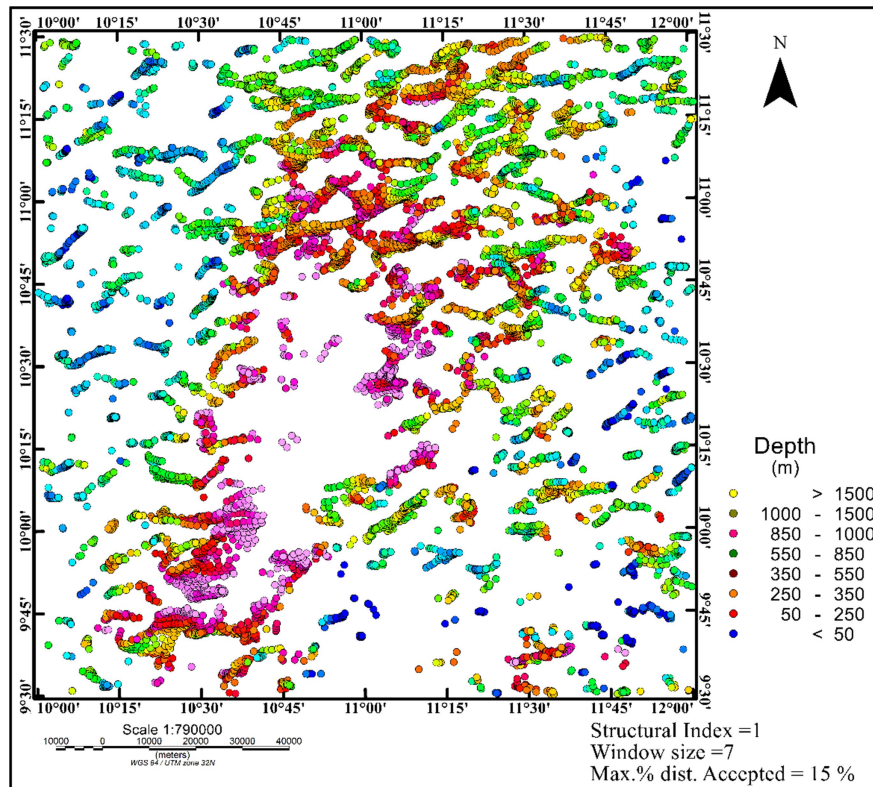

Figure 6. Euler Depth map of the study area showing estimated depths and structural lineaments distribution pattern.

3-2-7. Electrical resistivity sounding

A total of 60 vertical electrical sounding (**VES**) points were acquired in the study area (Appendix B, Figure 3). Hydraulic parameters such as aquifer transmisivity, hydraulic conductivity, and the existing boreholes yields were calculated and used to validate the groundwater prospectivity map created for the present area. Schlumberger electrode array was the method used in acquiring these **VES** data. The method involves the use of two current electrodes (**A**, and **B**), and two potential electrodes (M, and N). The field procedures involve the physical adjustments (expansion) of current electrodes while maintaining the potential electrodes at a fixed distance. Electrical current is normally being passed through the two current electrodes (**A** and **B**) each time the measurement is going to be taken. Concurrently, the potential electrodes measures the potential difference recorded within the depth of the measurement (Probe). The measured potential difference provides a measure of the resistance offered between the points of measurements. The measured resistance is also influenced by the geometrical configuration of the electrodes (Dobrin, 1976). While taking the measurements, the terrameter used was placed at the center of the potential electrodes **M** and **N**. A connecting cable was used to connect the points **M**, and **N** to the terminals **P1** and **P2** on the terrameter. However, the current electrodes were connected to the terminal points labeled as **C1** and **C2**. Measurements were taken after varying **AB/2** from 1 to 200 m.

3-2-8. Computation of Hydraulic parameters

The relationship between longitudinal unit conductance (Si) and transverse resistance (Ti) was first provided by Maillet (1947) as shown below:

$$S_i = \frac{h_i}{\rho_i} \tag{4}$$

$$T_i = h_i \rho_i \tag{5}$$

where ρ_i is the electrical resistivity, while h_i is the thickness of the layer.

The longitudinal conductance (S_i) and the transverse resistance (T_i) were so calculated. The aquifer transmissivity (T_r), and the hydraulic conductivity (K) are related as shown by the expression below:

$$T_{r} = K\sigma R = Kh_i \tag{6}$$

where σ is the electrical conductivity (reverse of resistivity), R is the transverse resistance, S_i is the longitudinal conductance, and h_i is the aquifer thickness. The hydraulic conductivity (K) was calculated using the expression provided by Heigold et al. (1979):

$$K = (386.40)R_{rw}^{-0.93283} \tag{7}$$

where K = the hydraulic conductivity and $R_{rw}^{-0.93283}$ = the resistivity of the identified (interpreted) acquiferous layer.

3-2-9. Slope and drainage density map production

Information revealed by slope map enables an assessment of how geology affects topography of an area. Hence, the degree of steepness of a slope can be related to the resistance offered by an outcropping rock to the weathering agents. The slope map for the present work was computed by using the "spatial analysts (slope)" tool found in Arc Map of the ArcGIS software. The DEM image of the study area was used as the input data into the "slope" tool of the ArcGIS software for the slope calculation. The computed slope map was further re-classified according to the assigned weight using the "re-class" tool of the "Arc toolbox" found in Arc Map of the ArcGIS software.

The drainage network of the study area was generated using the DEM image of the study area as the input data. The spatial analyst tool of the Arc Map found in the ArcGIS software was used for the drainage network computation. The drainage network map generated was further subjected to drainage density calculation by using the kernel density Algorithm of the ArcGIS software. The drainage density map generated was also re-classified further into three classes according to their assigned weight value using the "re-class" tool of the ArcGIS software.   The generalized research work flowchart for the present study is shown in Figure 7 below.
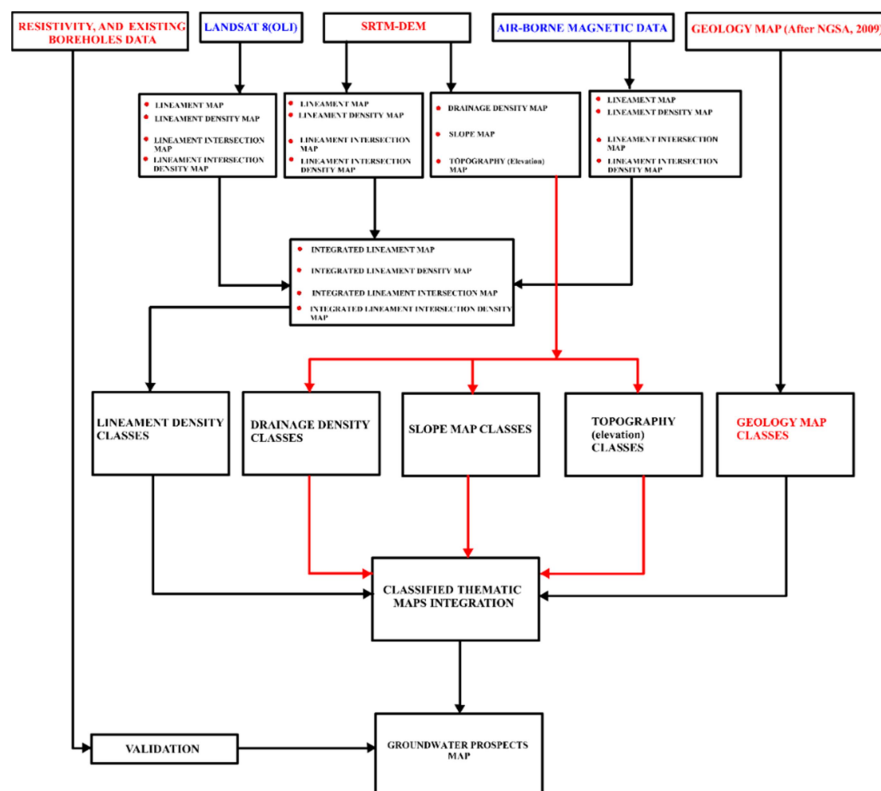
Figure 7. Research methodology flowchart.

4. Results and Discussion
4-1. Lineament maps

The results of lineament mapping exercise conducted on three different data types used are as presented in Figures 8, 9, 10, and, 11. Careful examination of these maps revealed the distribution of lineaments around different parts of the study area from the northern to southern and from western to eastern parts of the maps in a different directions (orientations) and density. On each of the delineated lineament maps, the lineaments could be seen to be oriented either in a NE-SW, NW-SE, N-S, or E-W directions. Moreover, visual observation of Figure 11-b shows that the various lineaments mapped from the different data types are intersecting each other in some areas, which is a very good phenomenon, as it is very significant in hydrogeological study, because it enables the percolation of water into the ground.

Furthermore, the visual examination of the lineaments distribution maps as well as their rose diagram plots (Figures 8-e, 9-e, 10-e, and 11-d) showed that the lineaments mapped from the different data sources have a dominant NE-SW pattern of the distribution. The study of the lineaments density maps (Figures 8-b, 9-b, 10-b, 11-b, and 12-d) showed the density of the lineaments mapped from each data type to be concentrated on different locations of the study area. For instance, the DEM-derived lineaments density map (Figure 8-b) shows the concentration of the mapped lineaments around western (Alkaleri, Darazo, areas), Central (Dukku, Nafada, and Bajoga areas), and the Southeastern (Kaltungo, Tula, Wuyo and Dadiya) parts of the study area. Moreover, considering the intersecting points of the DEM-derived lineaments (Figure 8-c), it could be seen that the intersecting points are denser (clustered) around the extreme southwestern, and the western parts of Alkaleri town, which is an area that is underlain by an outcrop of crystalline basement rocks (Figure 11-b). However, areas displaying moderate concentrations of the DEM-derived lineaments intersections points includes Wuyo, Tula, and Kaltungo areas.

Figure 8. DEM-derived; a) Lineaments distribution map, b) lineaments density map, c) lineaments intersection map, d) lineaments intersection density map, e) Rose diagram plots for DEM-derived lineaments distribution.

The Landsat-derived lineaments density map (Figure 9-a and 9b) shows the concentration of its mapped lineaments to be around the eastern parts of the study area. This area is represented by an elongated N-S trending lineament density anomaly that stretches from Nafada/Bajoga towns in the northeastern part of the study area, to the Wuyo, Tula, and Lamurde areas in the Southeastern parts. Moreover, areas displaying the most dense Landsat-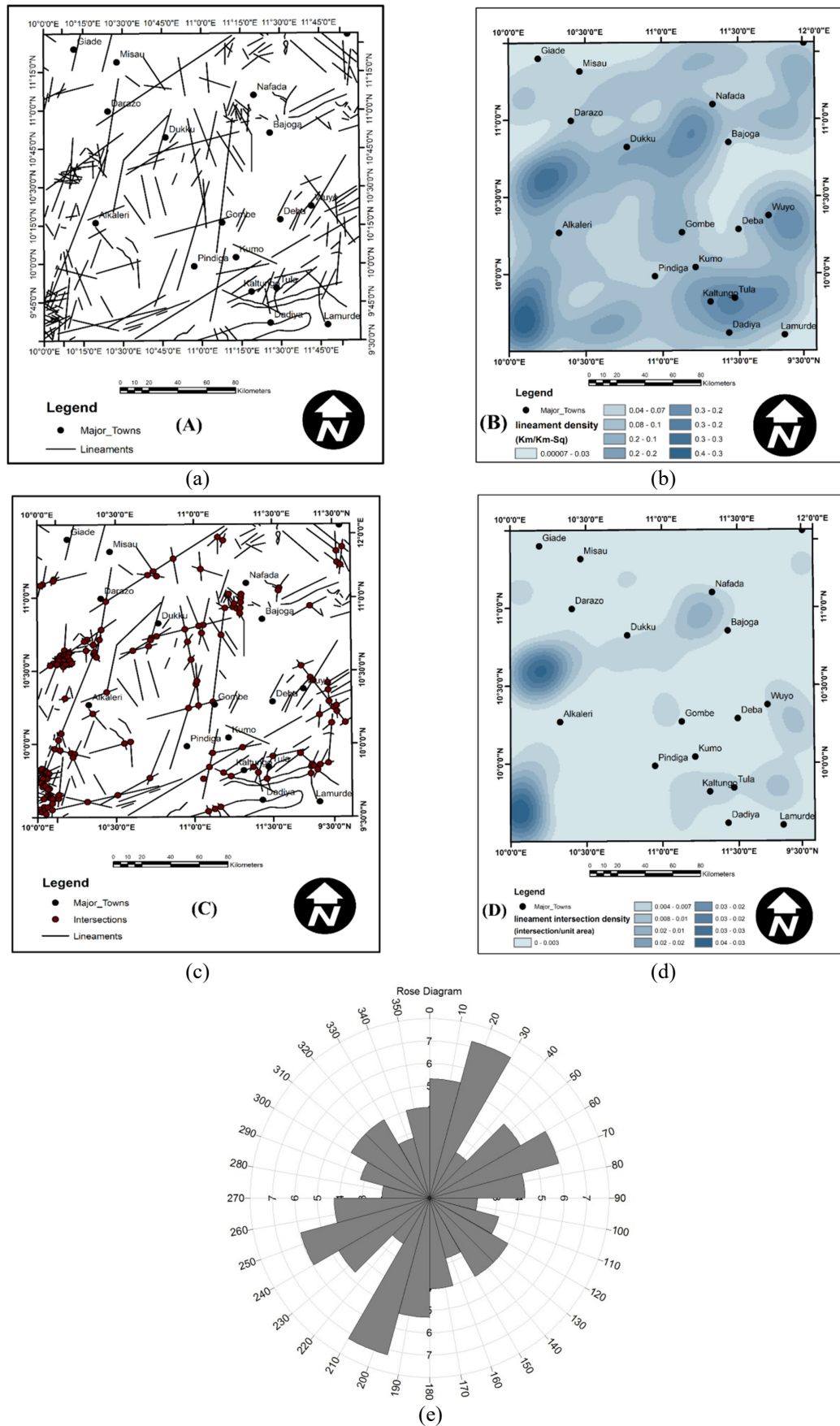derived lineaments intersections (Figure 9-c and 9d) are the elongated, N-S oriented anomaly (0.0097- 0.022 km/km^2) that runs from Nafada/Bajoga areas (in the northeastern part) to the Wuyo, Tula, and Lamurde areas (in the southeastern part) of the study area. Other areas that displayed higher density of the intersecting lineaments are Misau, Darazo, and the extreme southwestern parts of the map.

An observation of the magnetic derived lineaments distributions (Figure 10-a) and their distribution density maps (Figure10-b) shows the distribution and the clustering (concentrations) of these lineaments to be scattered (random) around Darazo, Dukku, Nafada, Bajoga, Wuyo, and Deba areas. One prominent area that displayed the greatest density of the magnetic-derived lineaments is Wuyo town and environs. The area is underlain by the outcrop of granitic and basaltic rocks (Figure 10-b). Furthermore, Figure 10-c and Figure 10-d shows the intersections and magnetic-derived lineaments intersection density maps with the greatest point of lineaments intersections to be around Wuyo, Deba, Gombe, Kumo, and Nafada/Bajoga areas. Other areas showing the greater density of the magnetic-derived lineaments are Darazo, Dukku, and Alkaleri areas. These are partly basement/sedimentary in nature (Figure 10-b).

The integrated lineaments distribution map (Figure 11-a), integrated lineaments density map (Figure 11-a) integrated lineaments intersection map (Figure 11-b), and the integrated lineaments intersection density map (Figure 11-c) provide a summarized view of the structural pattern, and distribution of the three data source-derived lineaments over the study area. The composite lineament distribution map (Figure 11-a) shows the integrated linear structures to

be oriented in different directions, with the dominant orientations (directions) found to be in NE-SW pattern (Figure 11-d), which is in agreement with the dominant strike direction of the Benue trough (Abdullahi et al., 2019). The integrated structures (lineaments) are further found to be at some locations, with the greatest points of their intersections found to be around Wuyo, Gombe, extreme southwestern part of Alkaleri areas. The integrated lineament density map (Figure 11-a) revealed the following locations in both crystalline basements and sedimentary locations to be having the greatest cluster of lineaments occurrence. These include Wuyo, Gombe, Deba, Kaltungo, Tula, and Pindiga areas.

4-2. Slope map

A slope is a measure of the degree or percentage rate of variation in height across a surface area (Manjare, 2014). The slope of an area controls the degree or percentage rate of the infiltration of water into the ground either positively or negatively. Gentle to flat slopes usually enhance the infiltration better than steep or high slope areas. The high/steep slope areas usually enhance the run-off, as it does not allow the water to stay on it any longer. According to International Mission for Sustainable Developments (IMSD), the slope of an area can be classified into nearly flat level (0° - 5°), very gentle (10° - 15°), gentle (15° - 25°), moderate (25° - 35°), strongly slope (35° - 60°), very steep slope (61°- 90°). However, for the purpose of this work, Figures 12-a and 12-b show the slope distribution map of the present area of study showing four classes (Table 3) with two classes: very gentle – flat slopes (0° - 18°), and very steep slopes (55° - 90°) being prominent and visible at Figure 12. The deep blue colored parts of the classified slope image map of the area represent very gentle to flat slope parts, while the greenish colored parts represent the very steep slopes part of the study area. The very gentle to flat slope parts of the study areas are found to be scattered around the study area (Figure 12), an elongated north-south very gentle to flat sloping area is found around the eastern part (between Bajoga and Wuyo areas) of the study area. This could probably be the location of the prominent Dadin-kowa dam

found near Deba town of the study area. This area that is the largest flat terrain in the region could enable the highest rate of ground water infiltration and accumulation. The greenish colored parts found at almost all parts of the study area represent zones of low groundwater recharge, as well as areas with high run-off.

4-3. Lithology map

The distributions (occurrence) and transmission of groundwater is significantly related to the porosity and permeability of the rocks interacting with the water (Sreedher et al., 2009). Usually, rocks with high porosity properties retain groundwater much better than their low porosity counterparts. Moreover, the permeability of a rock determines the ability of a rock to transmit the water through it. In other words, it determines the yields of the aquifer. Therefore, rocks with higher permeability transmit (yield) groundwater much better than their low permeability counterparts.

The geology of the present study area comprises of Precambrian basement rocks, cretaceous sedimentary successions and the volcanic rock outcrops (Figure 1). Massive and unfractured rocks (Figure 13a, 13b) (e.g. crystalline basements rocks) are normally found to have enhanced the run-off due to their low porosity, low permeability. Their porosity and permeability are only enhanced when they are highly weathered and fractured. On the other hand, areas with sedimentary or other porous rock materials usually show low run-off (high infiltration), e.g. the Bima sandstones, Yolde Formation, Gombe Formation of the study area. Volcanic rock outcrops also allows high or low infiltration of water depending on the degree of fracturing and the interconnectivity of the fractures within them. For instance, the Biu basalts outcropping at the extreme eastern part of the study area that shows a lot of columnar jointing pattern tends to allow only minimal run-off (has high infiltration rate).

4-4. Drainage density map

Drainage density pattern of an area is one of the very important factors of hydrogeological significance, as it reveals both surface and sub-surface formation information (Prasad et al., 2007). Drainage density is inversely related to the permeability. Hence, areas of high drainage density are attributed to low porosity and consequently low rate of infiltration (recharge). Whereas, areas of low drainage density corresponds to high porosity and consequently high groundwater recharge rate (Jaiswal et al., 2003; Murthy, 2000). However, other studies show that not all high drainage density zones are attributed to low infiltration rate or low recharge rate. For instance, studies by Shaban et al. (2005) and Sener et al. (2005) show some deviations from the earlier findings.

Figures 13-c and 13-d revealed the drainage density pattern of the present area of study. Careful observation of this map shows the distribution of the drainage density of the area to be in three classes that include; low, moderate, and high density areas. Areas with the Pinkish colored classes found near Nafada, Bajoga, Kaltungo, Misau, and Deba areas of the map shows high drainage density distribution as such it was classified as low potential zone. This is due to the fact that high drainage density areas usually promote (enhances) the surface run-off, and at the same time, prevent or slow down the surface water infiltration. However, locations displaying the greenish colored anomalies in the study area represent zones of moderate drainage density. These areas are classified as having a moderate potential in terms of the ground water storage capacity, because it can allow moderate level of surface water infiltration. Other areas represented by the yellowish colored anomalies represent low drainage density parts of the study area, and they are therefore classified as high potential class due to the fact that it allows more surface water infiltration, which can also go a long way in enhancing the ground water recharge.

(a)

(b)

(c)

(d)

(e)
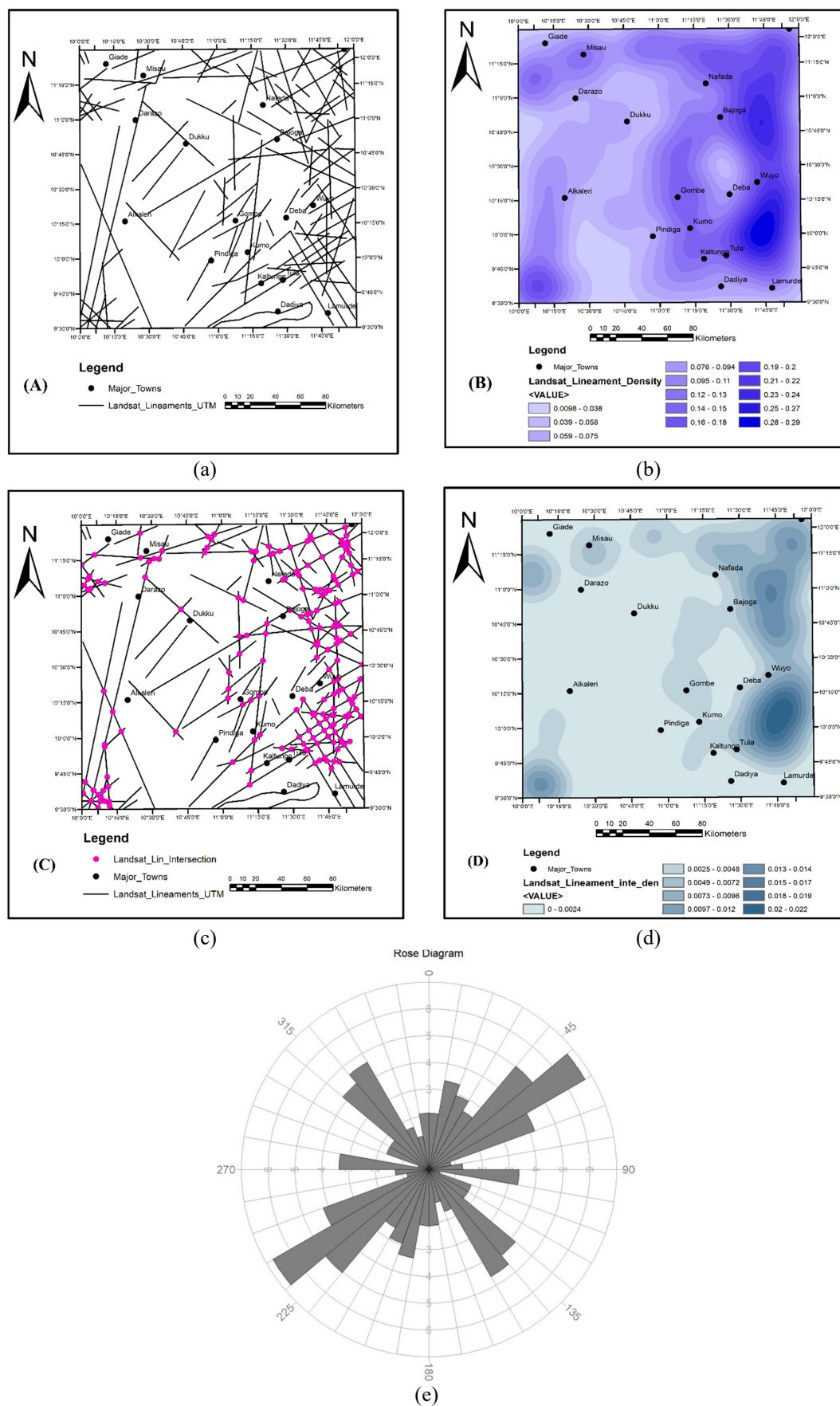
Figure 9. Landsat-derived; a) Lineaments distribution map, b) lineaments density map, c) lineaments intersection map, d) lineaments intersection density map, e) Rose diagram plot for the Landsat derived lineaments distributions.

(a)

(b)

(c)

(d)

(e)
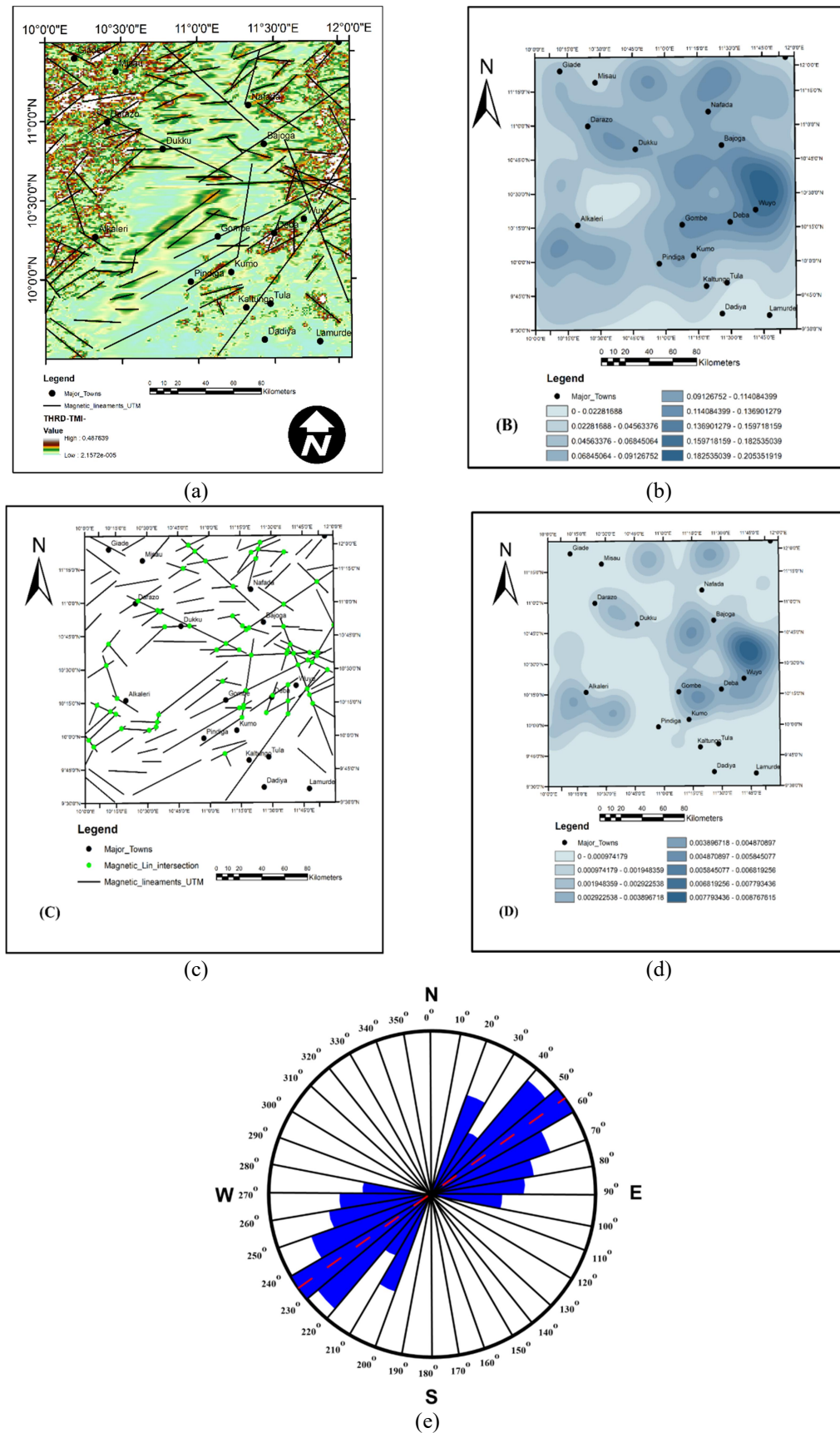
Figure 10. Magnetic-derived; a) Lineaments distribution mapped on total horizontal derivatives map, b) lineaments density map, c) lineaments intersection map, d) lineaments intersection density map, e) Rose diagram plot for the magnetic derived lineaments distributions.

(a)

(b)

(c)

(d)
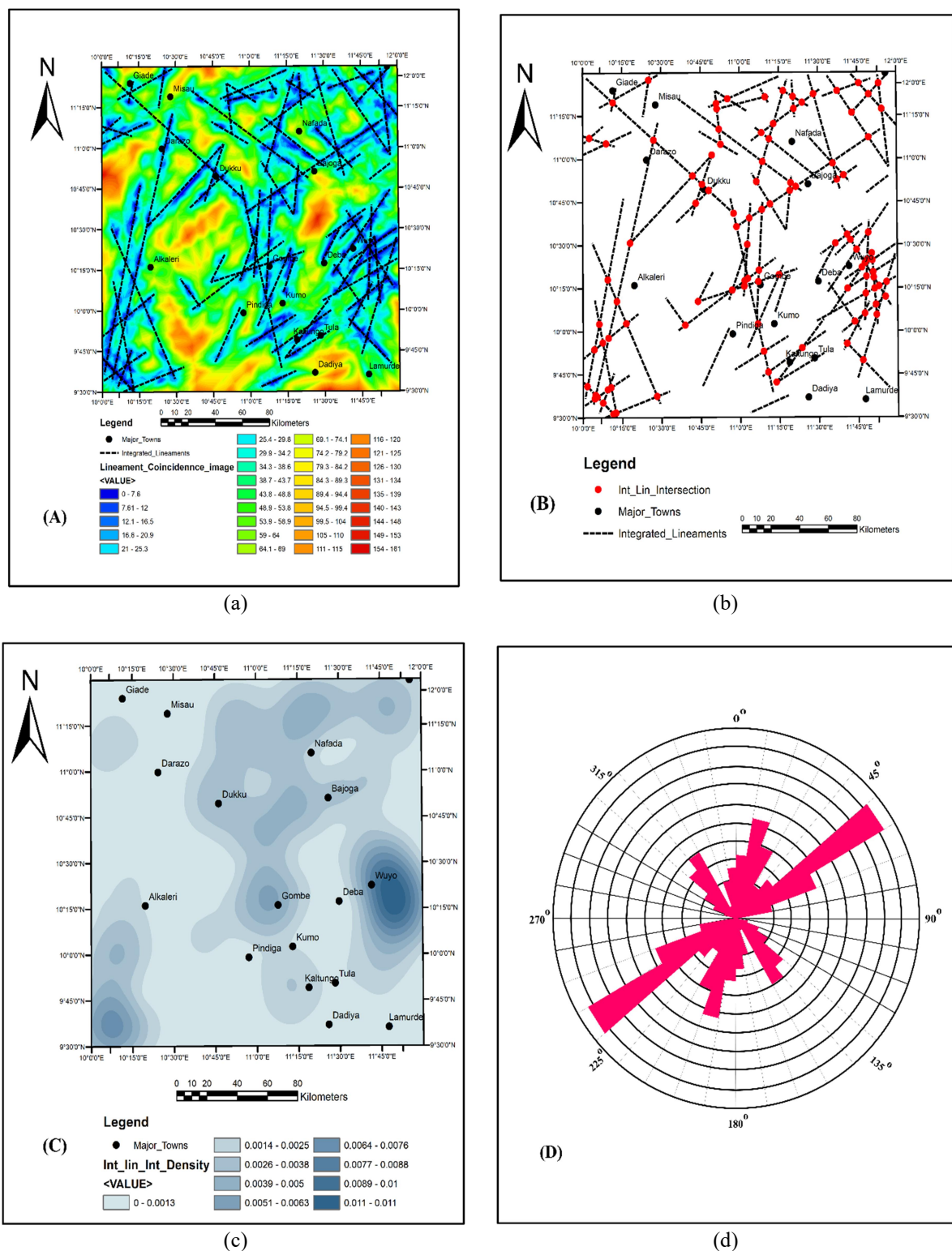
Figure 11. Integrated a) lineaments map, b) lineaments intersection map, c) lineaments Intersection density map, d) lineaments rose plot pattern of the study area.

(a)

(b)

(c)

(d)
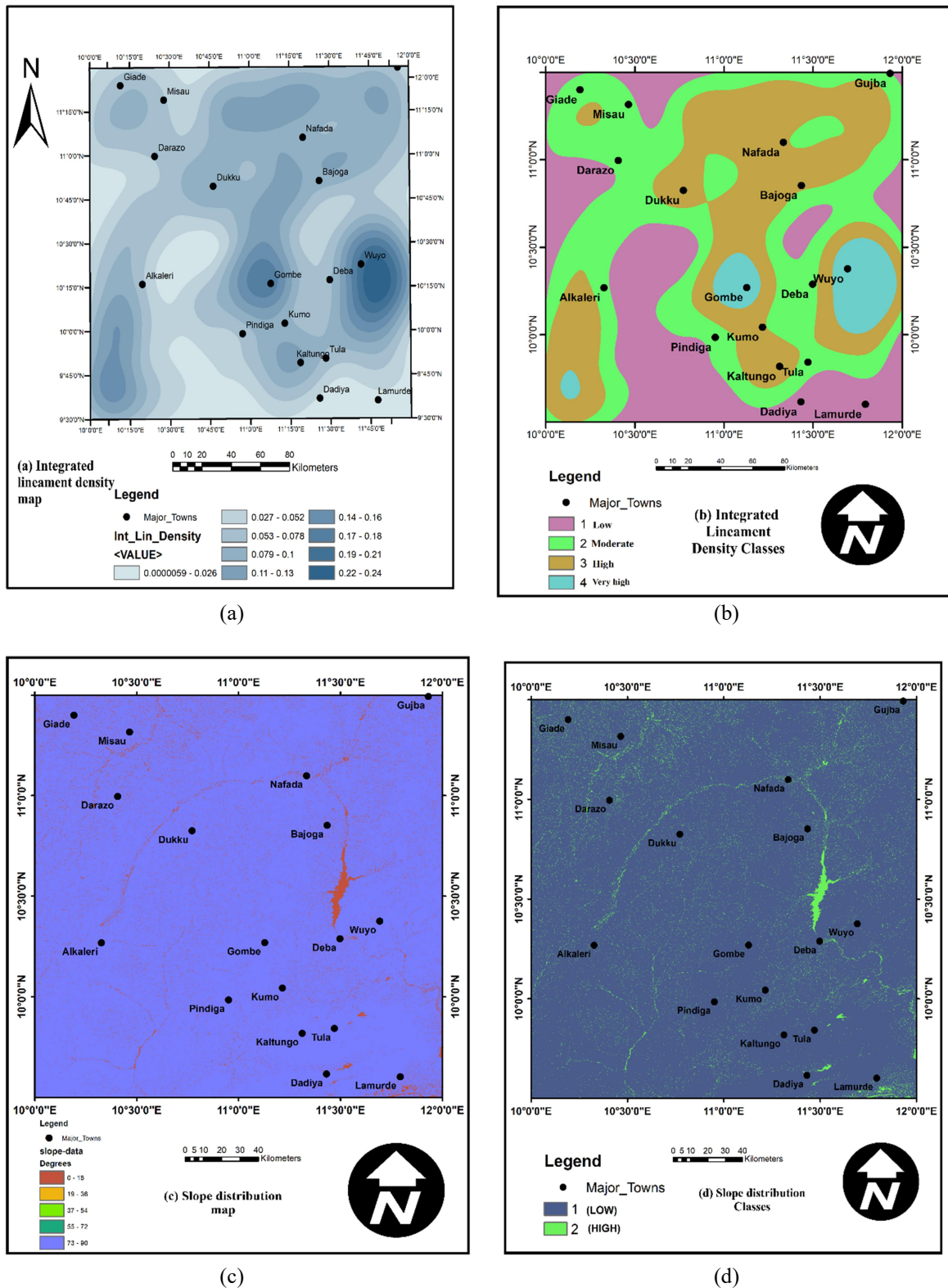
Figure 12. Thematic maps; a) integrated lineament density maps, b) integrated lineament density map classified according to its assigned weight, c) DEM-derived slope map, d) Slope classes' map.

(a)

(b)

(c)

(d)
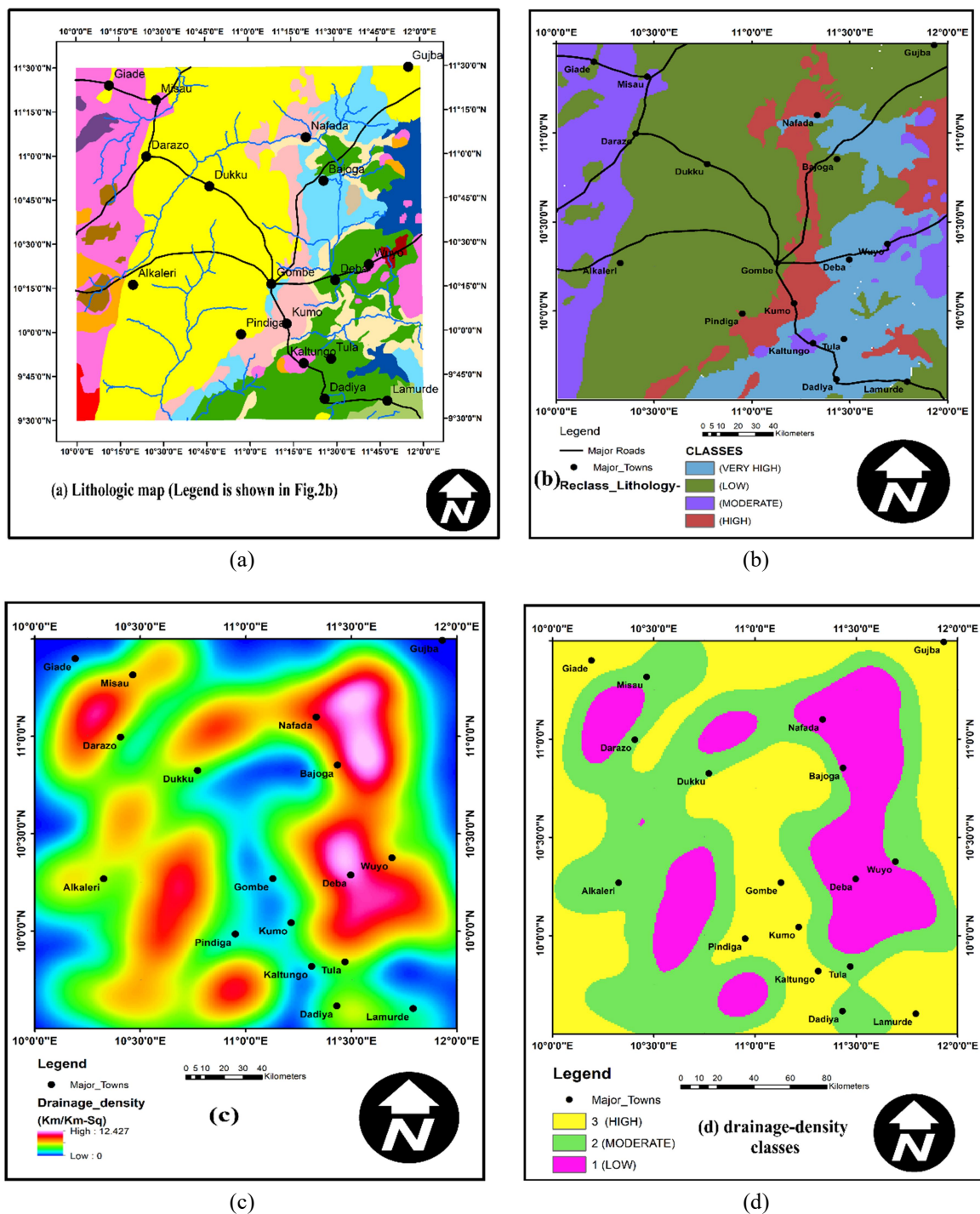
Figure 13. Thematic maps; a) Geology map modified after NGSA, 2009, b) geologic map classified according to its assigned capability of storing groundwater, c) drainage density map, d) drainage density class map.

(a)   (b)
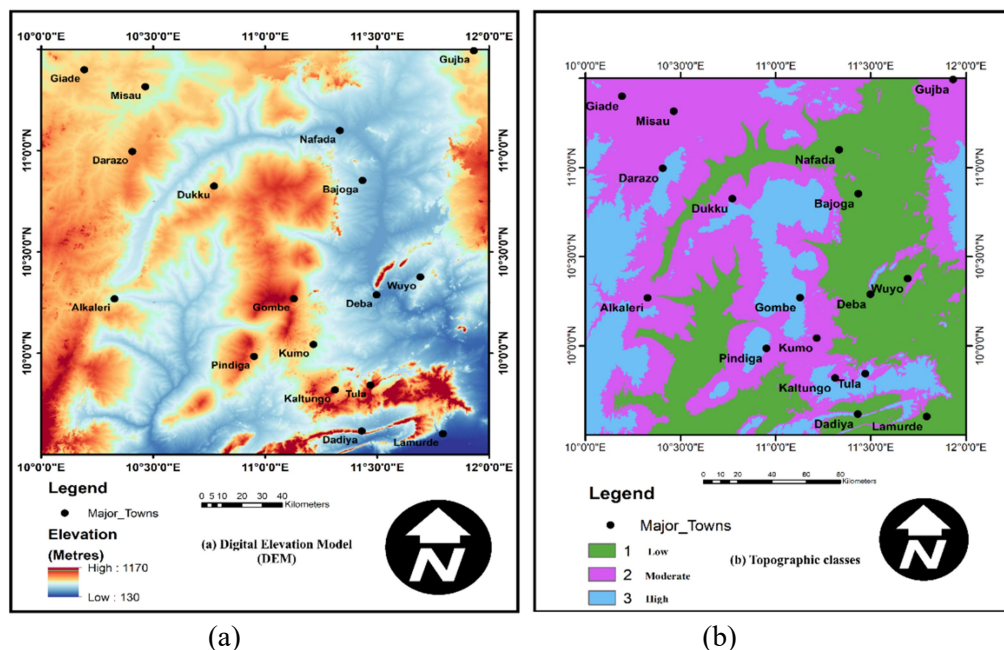
Figure 14. Thematic maps; (a) digital elevation model map showing the topographic relief of the study area, (b) topographic map classified according to the assigned weight depending on degree of influence of each thematic layer class to groundwater occurrence.

4-5. Geomorphology (topography) map

A ground surface morphology that includes hills, valleys, plains, plateaus, and other surface topographic features are considered and selected as one of the important criteria that contributes to the ground water occurrence. This is because the movement of surface water on high or low altitude terrains has some degree of influences on the surface water infiltration and recharge. The differences in elevation between two areas on the earth surface usually bring about the slope in an area, and slope determines the direction of surface water flow usually form a highly elevated zones to low topographic terrains (Abdalla, 2012). Hence, the downloaded SRTM-DEM data was used in re-classifying and the subsequent analysis of the different surface morphology of the study area.

The study shows that the surface elevation is in ranges of 100 m to 1000 m (above the sea level). The availability of highly elevated and low elevated areas provides the avenue for the movement of the surface water to areas with depressions (areas of low elevations). It can be seen from the re-classified DEM map of the study area (Figure 14-b) that the areas around Alkaleri, Darazo, Misau, Dukku, Wuyo, Kaltungo and Tula towns are highly elevated as such surface run-off is more on those areas compared to areas like Gombe, Deba, Nafada, Bajoga, and Pindiga towns. That serves as a low elevated area where a lot of infiltration (recharge) of the water is expected to be prominent (significant).

4-6. 3D Euler Depth Map

An observation of the 3D Euler depth solution map (Figure 6, above) shows the generated depth values to be distributed haphazardly. However, a further check on the map revealed the concentration of deeper structural lineaments depths around the central parts of the study area. Most of these deeper structures that include depth range of 850-1000 m, 1000-1500 m, to > 1500 m are dominant in the central parts of the map, which is an area that is mostly underlain by an outcrop of sedimentary Gongola basin. This implies that the structures mapped are actually the subsurface basement linear structures that are overlain by the sedimentary rock cover. Moreover, the distribution of shallower features whose depth range are from 550 – 850 m, 350 – 550 m, 250 -350 m, 50 – 250 m, to <50 m. These shallower sub-surface depth values could be attributed to the presence of near surface structural faults and fractures that could be found at near surface basement, and volcanic rocks outcrops. The major trends of the

structures mapped is the NE-SW pattern.

4-7. Geo-electrical Parameters

The electrical resistivity survey data obtained was used to interpret the primary geo-electric parameters using a win-resist 2 software. Parameters such as the number of layers, apparent resistivity of the layers, thicknesses of the layers, depth, curve types, and the inferred aquifer system were identified, interpreted and presented at Appendix A. A total of 13 curve types were found across all the VES points interpreted and presented in Appendix A. These includes: KHK, KHA, HKH, HK, QQ, AK, AKH, KQH, QHA, HA, QH, AA, and KQ. The three geo-electric sections drawn reveals a range of layers that varies from 5 to 4 across the VES points used (Appendix A).

The first lithological layer appearing across all the VES points and boreholes is referred to as the top soil layer. This layer comprises of loose sands and clayey soil. It also has layer resistivity and thicknesses that ranges from 725.9 Ωm to 15.2 Ωm, and 12.7 m to 1.0 m, respectively.

The second lithological layer identified comprises of clayey sand (in most of the locations), and silty-shale in certain locations. The layers resistivity as well as thicknesses values ranges from 502.9 Ωm to 0.6 Ωm respectively.

The 3rd lithological layer identified comprises of medium grained sandstones, siltstones, and ironstones/mudstones in some few locations such as V 42, V 22, V 36, V 9, and borehole no.44 among many others. The layer is characterized by resistivity that ranges from 742.1 Ωm to 12.5 Ωm, and a layer thickness that ranges from 52.6 m to 9.7 m.

The 4th lithological layer is composed of siltstone, silty shale, sandy clay, kaolinated sand and claystone depending on the location. Certain locations such as V 05, V 09, , V 08, V 22, and V 27 show the presence of a 5th lithological layer that includes claystones, and silty shale.

4-8. Aquifer systems

A total of six boreholes and 14 VES points distributed in the study area were used in correlating the Vertical Electrical Sounding (VES) interpretation with the boreholes lithological sections along the three major profiles drawn at different trends on the location map of the study area (Figure 3).

A profile line A – A' drawn on the study area map (Figure 15) in a NE-SW pattern encountered two boreholes (B 9, and B 44) and 4 VES points (V 42, V 36, V 22, and V 09). After the lithological correlation with the VES points along profile A - A'. A unique layer identified as acquiferous is a medium grained sandstone layer. This layer is characterized by resistivity and thickness that ranges from 112.8 Ωm to 47.1 Ωm, and 42.8 m to 19.1 m. Underlying the acquiferous layer in boreholes B 44, and VES points (V 42, V 22, and V 09,) is a silty shale layer. A siltstone lithology layer was found to emerge at V 09, and B 09 as layer 3 with a corresponding thickness of 35.6 and 6.0 m respectively.

A sandy clay layer overlying the medium grained sandstone at V42, disappeared in the remaining VES points and borehole lithology. This could be due to the impact of tectonic events that led to the folding and faulting of most of the sedimentary rocks in the Benue trough (Giraud and Maurin, 1992; Obaje, 2009; Nwajide, 2013). Moreover, the ironstones/mudstone found beneath the clayey sand layer at V 22, disappeared in the remaining VES points and the corresponding borehole lithological logs. A further study of the profile section (Figure 15) reveals the aquifer type delineated to be semi-confine to confine in nature.

A profile labeled B – B' is drawn along a NW – SE pattern on the study area (Figure 16) and passes through two boreholes and four VES points that includes V 51, V 38, V 37, V 35, and boreholes B 24 and B 53. The interpreted VES point were compared and correlated with the available boreholes lithology logs. The medium gained sandstone layer (the acquiferous layer identified) has a thickness in a range from 43.2 m to 23.6 m (Figure 16).

The Siltstone lithology being the 3rd layer found at borehole 37 did not appear at the other VES points. The siltstone lithological layer appeared at VES 37 with a thickness of 14.9 m. The aquifer type identified is confine to semi-confined.
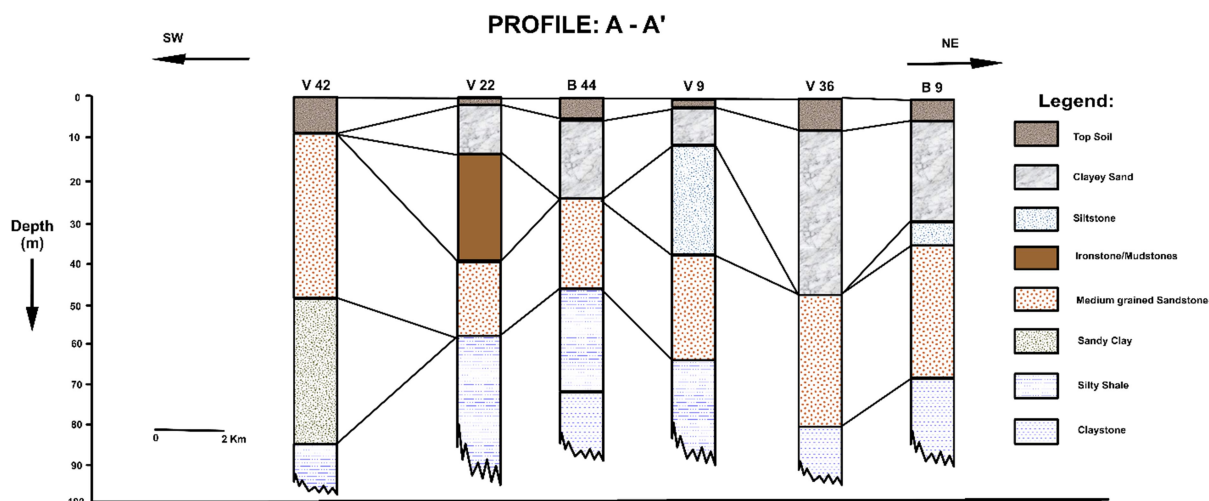
Figure 15. A Profile A –A' taken along SW – NE pattern on the location map of the study area.
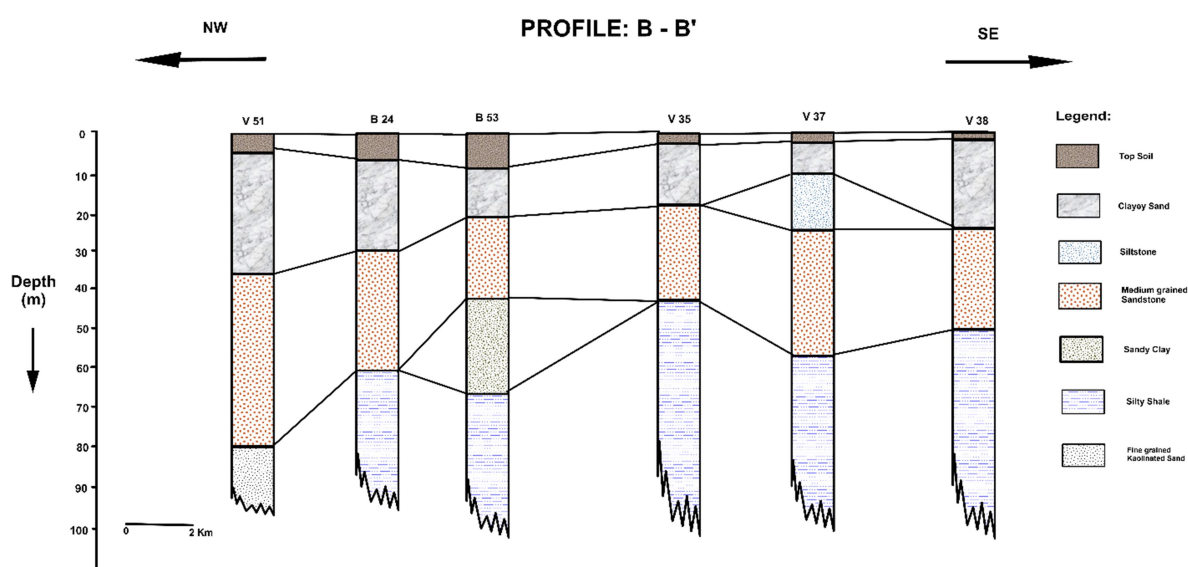
Figure 16. A Profile B –B' taken along NW – SE pattern on the location map of the study area.

A third profile labeled as C – C' is drawn along a NE – SW trend on the location map of the current research area (Figure 17). The profile passes through two boreholes (B 55, and B 48), and six VES points (V 27, V 24, V21, V 11, V 8, and V 19). The two borehole lithologs were correlated with the other VES points in the section. The acquiferous layer identified in this section is the same medium grained sandstones. The medium grained sandstones have a thickness that ranges from 35.2 m to 21.4 m. the siltstone lithology found as layer 3 in V 27 did not appear in the remaining other VES points and other

boreholes penetrated by the section. Moreover, ironstone/mudstone layer appeared at V 21, V 11, and B 55. It however did not appear at V 8, V 27, V 24, V 8, V 19, and B 48.

On a generate note, the appearance and disappearance of certain lithologies across the different VES points and boreholes found at the study area can be attributed to the numerous faulting and folding activities that occurred during the past tectonic events especially the Santonian orogeny that affected most parts of Benue trough (Obaje, 2009). The identified aquifer system here is a semi-confine to confine in form.
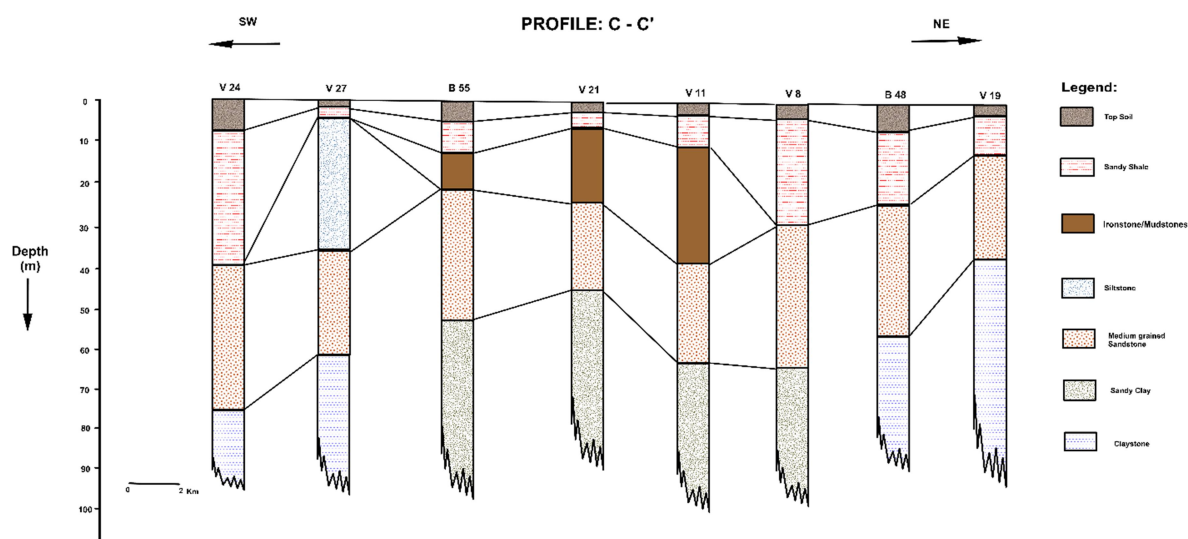
Figure 17. A Profile C –C' taken along NW – SE pattern on the location map of the study area.

4-9. Aquifer Transmisivity, Hydraulic Conductivity, and Bore hole yields

The Transmisivity values for the acquiferous layers were calculated by Equation (6) after Todd (1980). The values are presented at Appendix B. An observation of the values presented in Appendix B shows variable aquifer transmissivities across different VES points. The transmisivity values calculated ranges between 849.13 m^2/day and 29.76 m2/day. The mean transmisivity value for the study area is 285.79 m^2/day. Further check on Table 2 shows the highest aquifer transmisivity value of 849.13 m^2/day was recorded at VES 56, which is located at Guyuk town. A minimum transmisivity value of 29.76 m^2/day was also recorded at VES 47 situated around Duggal Zange town of the study area. The Transmisivity values calculated at each of the VES points and for each of the acquiferous layer was classified according to the Offodile (1983) aquifer transmisivity classification scale (Table 2), and the result is presented at Appendix C. A closer check on Appendix C shows a total of 13 VES points belonging to a high aquifer transmisivity class. These aquifers are found at VES 03 , 05, 10, 15, 20, 23, 35, 38, 44, 55, 56, and 60. Whereas, the remaining 47 VES points belong to an aquifer transmisivity class that is moderate in nature. The high transmisivity aquifer layers constitute about 21.67% of the total VES points examined, while, the remaining aquifers displayed moderate transmisivity values that constitutes

78.33% of the total VES points studied.

The hydraulic conductivity values computed for the entire 60 VES points were determined from Equation (8) provided by Heigold et al. (1979). An observation of the values presented at Appendix C shows the maximum and the minimum values of 48.262 m/day and 1.37 m/day recorded at VES 35, 44, and VES 50 of the study area. The average hydraulic conductivity values calculated for the entire VES points was found to be 11.068 m/day.

Borehole yields from 67 boreholes that are randomly distributed at different locations of the study area (Figure 3) were measured directly from the existing wells. Information such as borehole depth (m), static water levels (m), draw down (m), discharge rate (l/s), and finally the well yields (Liter/min.) were obtained for each well. The result is presented in Appendix D. A careful examination and analysis of the result shows the borehole yield obtained varies across the 67 wells used. The yields varies from high (93.75 L / min.) to low (25.0 L/min.). The highest yield value of 93.75 L/min was obtained at well 10 at Garin Gado town as shown in Figure 3. However, well no 66 has the lowest value of the groundwater yield in the study area. Furthermore, the entire borehole yields measured across all the available boreholes used were grouped into four classes with the following range of values defining each class as presented below:

Table 1. Borehole yield classification for the study area.

Range (Liter/minutes)	Yield:	Remark:
< 39	Low yield	Low potential
40 - 49	Moderate yield	Moderate potential
50 - 59	High yield	High potential
> 60	Very High yield	Very High potential

Hence, 24 wells out of the total of 67 boreholes whose yields were measured were found to have yields greater than 60 Liters/minutes (Appendix D), as such, they are classified as very high yield/ very high potential wells. However, 23 of these wells have groundwater yields that ranges from 50 to 59 liters/minutes, hence they are classified as a high yield/ high potential wells. A total of 14 boreholes whose measurements were taken reveals that they are in a moderate yield/ moderate potential class. This is due to the fact that their measurements falls within the aquifer yields of 40 -49 liters/minutes range. The remaining six boreholes found in the study area has aquifer yields that are less than 39 liters/minutes. Therefore, they are classified as low yield/ low potentials bore holes.

4-10. Groundwater prospectivity map
Developments of groundwater prospectivity map of an area are considered to be very imperative in terms of the planning and development of clean and sustainable water supply for domestic and industrial usage. Hence, the groundwater potential map of this area was produced by integrating each thematic map like: slope, lithology, topography (landforms), integrated lineaments density, and drainage density pattern of the study area (Figure 9, 10, and, 11). The above-mentioned maps were integrated using GIS technique.
The categorization of groundwater prospective zones was done on the basis of the integration of multiple criteria such as landforms, slopes, lithology, integrated lineament density, and drainage density (Sikdar et al., 2004; Jasrotia et al., 2007; Mohammed-Aslam et al., 2010; Abdalla,

2012). This process involves the assignment of weight values to each of the thematic maps used on the basis of their influence on the storage of groundwater (Table 3). The rank of each thematic map divided by the total sum of ranks for the individual maps gives the thematic layer weight (**TW**) values for each of the maps. Similarly, the maps classes were assigned different ranks depending on the degree of influence of each map layer with respect to its groundwater storage capacity. The classes were ranked between 4 and 1, with 4 being the most influential layer in terms of the groundwater storage, while 1, being the least in terms of its groundwater storage ability. The capability values (**CPV**) for each of the layer classes was obtained by dividing the individual layer rank by the total sum of all the individual layer's ranks used. The earlier calculated thematic layer weight (**TW**) values were then multiplied by their respective capability (**CPV**) values to obtain the groundwater prospectivity map of the study area (Figure 18) using "Spatial Analyst tool" of the ARC GIS environments. This process is expressed mathematically as:

$$GRWP = \sum TW \times CPV \qquad (8)$$

where **GRWP** stands for groundwater potential or prospects, **TW** stands for map weight, and the CPV stands for the capability values for each map class.

$$GRWP = \sum TW \times CPV \ (for; DRD, LND, SLP, LTH, TPG) \qquad (9)$$

where **DRD** represents the drainage density, **LND** represents the integrated lineament density, **SLP** represents the slope map, **LTH** represents the lithology, and **TPG** represents the topography (landforms).

Table 2. Aquifer transmisivity classification after Offodile (1983).

Aquifer Transmisivity (m^2/day)	Well Classification
>500	High potential
50 - 500	Moderate potential
5 - 50	Low potential
0.5 - 5	Very low potential
< 0.5	Negligible potential

The groundwater prospectivity map (Figure 18) produced shows the distribution of groundwater occurrences of the study area. The map was categorized into low, moderate, high, and very high prospects or potential zones. Areas displaying very high groundwater prospects as shown in Figure 18 are represented by brown-colored anomalies. They include locations around Gombe, Wuyo, Bajoga, Nafada, Tula, Kaltungo, Misau, and parts of Alkaleri town. On the contrary, locations showing low groundwater prospects (blue- colored parts) are found to be near Lamurde, Giade, West of Pindiga, A location between Bajoga and Wuyo town, and an area located towards the west and south of Gombe and Dukku towns respectively.

The yellowish colored class of the prospectivity map represents areas having high groundwater prospects, whereas, the purple colored parts represents areas of moderate groundwater prospects. The areas displaying low, moderate, high, and very high ground water potentials are found to cut across all the three main geological terrain (Precambrian basements, sedimentary, and volcanic rocks) of the study area. What makes an area to be classified as low, moderate, high, and very high potential zone is the hydrogeological characteristics of the terrain around the area which includes its porosity and permeability, density of fractures (in case of crystalline zones), drainage density, slope pattern, as well as the topography (landforms) of the terrain.

The validation of this map was performed using the geophysical derived parameters such as aquifer transmisivity, hydraulic conductivity and the available borehole data (such as well yields). A careful observation of the groundwater prospectivity map (Figure 18) created shows a reasonable degree of consistency of the four main potential classes (very high, high, moderate, and low classes) with the spatial distribution of the calculated hydraulic conductivity, aquifer transmisivity, and the well yields measured from Vertical Electrical Sounding (VES points) results and the existing boreholes. Spatial distribution in most of the VES points showing high aquifer transmisivity values shows high degree of conformity with the areas mapped as high to very high potential class. This can be seen by the distribution of numerous VES points with high transmisivity values (such as; V 5, V 10, V 20, V 35, V 38, V 55, and V 60 among others) within the high to very high potential class. Moreover, the borehole yield information gotten from the numerous boreholes distributed in the study area (Figure 18) shows a reasonable level of the agreement with the groundwater potential classification map of the area. This can be observed when Figure 18 is examined. The most of the greenish colored wells that represent the high yield class boreholes (as shown in Figure 18) agrees spatially with the high to very high potential class generated. Other boreholes that show moderate yields also agree substantially withier corresponding groundwater potential class. Hence, the relative degree of conformity obtained has validated the groundwater prospectivity map produced for the current area.

Table 3. Thematic map assigned weight and layer capability values.

Thematic layer	Map rank	Map weight (*TW*)	Class ranges	Degree	Class rank	Class capability value (*CPV*)
Lineament density map	3	0.23	0.000006 – 0.046132	Low	1	0.10
			0.046132 – 0.084877	Moderate	2	0.20
			0.084877 – 0.139306	High	3	0.30
			0.139306 – 0.235247	Very High	4	0.40
Drainage density	3	0.23	0 – 3.362604	High	3	0.50
			3.362604 – 7.066342	Moderate	2	0.33
			7.066342–12.427015	low	1	0.17
Slope	2	0.15	0 - 18	Very High	4	0.40
			19 - 36	High	3	0.30
			37 - 54	Moderate	2	0.20
			55 - 90	Low	1	0.10
Topography	3	0.23	130 - 362	High	3	0.50
			362 - 491	Moderate	2	0.33
			491 - 1170	Low	1	0.17
Lithology	2	0.15	Bima Formation	Very High	4	0.15
			Yolde Formation	Very High	4	0.15
			Older Basalts	High	3	0.11
			Gombe Formation	High	3	0.11
			Med-coarse-grained granites	Moderate	2	0.07
			Banded gneiss	Moderate	2	0.07
			Migmatites gneiss	Moderate	2	0.07
			Porphyritic granites	Moderate	2	0.07
			Keri-Keri Formation	Low	1	0.04
			Alluvium	Low	1	0.04
			Pindiga Formation	Low	1	0.04
			Charnokytes	Low	1	0.04
			Ignimbrites	Low	1	0.04
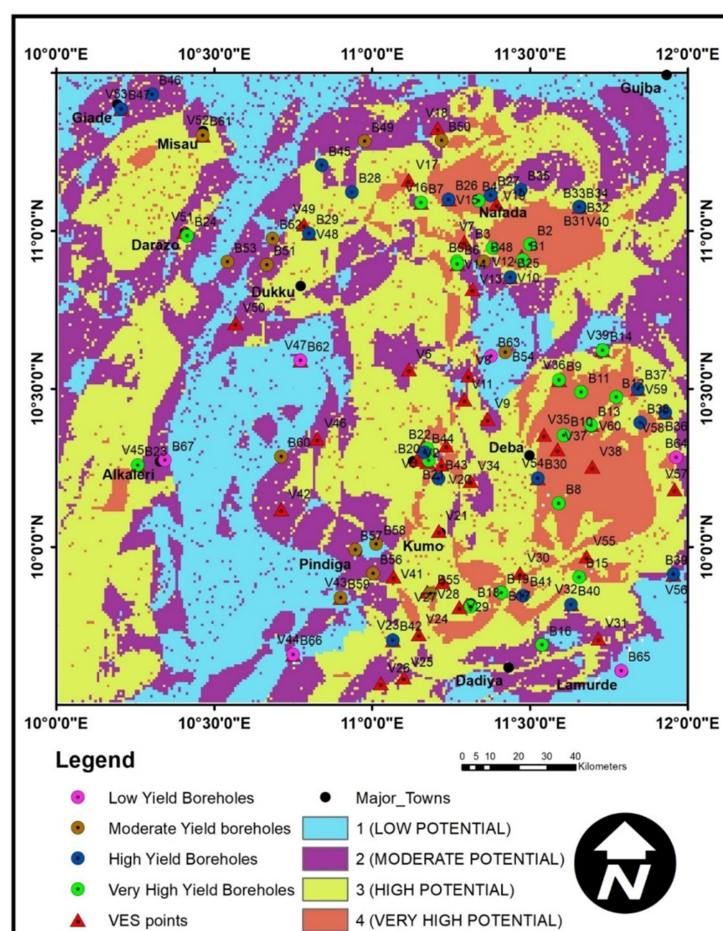
Figure 18. Groundwater prospectivity map of the study area, with existing boreholes and VES point distributions super imposed (Thompson, 1958).

5. Summary and Conclusions

The groundwater prospectivity map created for the study area through the application of GIS and remote sensing technique enables the successful mapping of various regions of favorable occurrence of groundwater. The integration of various thematic maps (slope, drainage, lineaments density, topography, and lithology) using GIS technique for Multi-Criteria Evaluation (MCE) of the groundwater prospects was successfully applied and validated using aquifer transmisivity, hydraulic conductivity, and well yields obtained from the electrical resistivity and existing boreholes data.

The classification of the groundwater prospect map into low, moderate, high, and very high prospective zones was achieved on the basis of the degree of the influence of each thematic map and layer class on the possible occurrence of the groundwater around the study area. The areas mapped as "very highly prospective" are areas that have very high probability of the groundwater occurrence and are found to be having high lineament density, high porosity and permeability, gentle-flat slope as well as low drainage density.

The distribution of the current existing boreholes shows that some of the locations of the current boreholes are within the moderate to highly prospective zones; as such their yield might be sufficient to support the needs of their immediate community. The present study also reveals some highly prospective zones, especially the western parts of the map that are yet to be explored.

The aquifer system identified for the study area after VES correlation with available borehole log is semi confine to confine in form.

* Appendices (A-D) are not printed but in a PDF file in the paper at Journal site.

References

Abdullahi, M., Singh, U.K. and Roshan, R., 2019, Mapping magnetic lineaments and subsurface Basement beneath parts of Lower Benue Trough (LBT), Nigeria: Insights from integrating Gravity, Magnetic and Geologic Data. Journal of Earth System Science., 1-7.

Abdalla, F., 2012, Mapping of groundwater prospective zones using remote sensing and GIS Techniques: A case study from Central Eastern Desert, Egypt. Journal of African Earth Sciences. 70, 8-17.

Abubakar, M.B., 2006, Biostratigraphy, Palaeo environment and organic geochemistry of the Cretaceous sequences of the Gongola Basin, Upper Benue Trough, Nigeria. Ph.D. Thesis, Abubakar Tafawa Balewa University, Bauchi, Nigeria. 139-140.

Ahmed, II.J.B., and Mansor, S., 2018, Overview of the application of geospatial technology to Groundwater potential mapping in Nigeria. Arabian Journal of Geosciences. 11, 504.

Ahmed, II.J.B., Okunlola, I.A, Abdullahi, I.N. and Kolawole, L.L., 2013, Assessment of effects of Abattoir activities on groundwater quality in part of Keffi, North Central Nigeria. Water Resources 23, 72–91.

Chuma. C., Orimoogunje, O.O.I., Hlatywayo, D.J. and Akinyede, J.O., 2013, Application of remote sensing and geographical information Systems in determining the groundwater potential in the crystalline basement of Bulawayo metropolitan area, Zimbabwe. Advance Remote Sensing 2, 149–161.

Cordell, L. and Grauch, V.J.S., 1985, Mapping basement magnetization zones from Aeromagnetic Data in the San Juan basin, New Mexico, in W. J. Hinze, ed., the utility of regional gravity and magnetic anomaly maps: SEG, 181-197.

Dobrin, M.B., 1976, Introduction to Geophysical prospecting. Third edition. McGraw-Hill, New York. 89 – 97.

Epeju, J., Olasehinde, P.I., Okhimamhe, A. and Okunlola, I. A., 2017, Investigation of Hydrogeological structures of Paiko region, north-Central Nigeria using

integrated geophysical and remote sensing techniques. Geosciences (Switzerland) 7, 1–17.

Elbeich, S.F., 2014, An overview of integrated remote sensing and GIS for groundwater Mapping in Egypt. Ain Shams Engineering Journal 6(1), 1–15.

El-Naqa, A., Hammouri, N., Ibrahim, K. and El-Taj, M., 2009, Integrated Approach for Groundwater Exploration in Wadi Araba using remote sensing and GIS. Jordan Journal of Civil engineering, 3(3).

Elbaz, F., 2008, Remote Sensing of the Earth: Implications for Groundwater in Darfur. Technologies for clean water. https://www. nae.edu/Publications.aspx (accessed on 15 March, 2016).

Fashae, O.A., Tijani, M.N., Talabi, A.O. and Adedeji, O.I., 2014, Delineation of groundwater potential Zones in the crystalline basement terrain of SW-Nigeria: An integrated GIS and remote sensing approach. Appl. Water Science. 4, 19–38.

Giraud, R. and Maurin, J. C., 1992, Early Cretaceous rifts of Western and Central Africa : an overview. Tectonophysics, 213, 153–168.

Hammouri, N., El-Naqa, A. and Barakat, M., 2012, An integrated approach to groundwater Exploration using remote sensing and geographic information system. J Water Resource Prot 4(9), 717–724.

Heigold, P.C., Gilkeson, R.H., Cartwright, K. and Reed, P.C., 1979, Aquifer Transmisivity from Surficial electrical methods. Ground water. 17 (4), 333 – 345.

Jasrotia, A. S., Kumar, R. and Saraf, A. K., 2007, Delineation of groundwater recharge sites using Integrated remote sensing and GIS in Jammu district, India. International Journal of Remote Sensing 28(22), 5019–5036.

Jaiswal, R.K., Mukherjee, S., Krishnamurthy J. and Saxena, R., 2003, Role of remote sensing and GIS Techniques for generation of groundwater prospect zones towards rural development-an approach. International Journal of Remote Sensing. 24, 993–1008.

Lovelyn, S. K., Hamidu, H., Mbiimbe, E. Y., Sidi, M. W. and Farida, G. I., 2016,

Suitability of Ground and Surface Water Resources for Different Uses in Boh Community Gombe State Northeastern Nigeria. Nature and science journal, 24.

Manjare, B.S., 2014, Identification of groundwater prospecting zones using remote sensing And GIS techniques in upper vena river watersheds Nagpur district, Maharashtra, India 15th Esri India User Conference 2014, 1–14.

Mboringong, M.N., Olasehinde, A., Tabale, R. P., Yusuf, A. and Ashano, E.C., 2013, Evaluation of Arsenic Concentration in Rocks of Kaltungo Area, Upper Benue Trough, Nigeria. Journal of natural sciences research 3(4), 25-30.

Mogaji, K.A., Aboyeji, O.S. and Omosuyi, G.O., 2011, Mapping of lineaments for groundwater Targeting in the basement complex region of Ondo state, Nigeria, using remote sensing and geographic information system (GIS) techniques. International Journal of Water Resources Environ Eng 3(7), 150–160.

Mohammed-Aslam, M. A., Kondoh, A., Rafeekh, P.M. and Monobaran, A. N., 2010, Evaluating Groundwater potential of a hard rock aquifer using remote sensing and geophysics. Journal of Spatial hydrology. 10 (1), 76 – 88.

Meijerink, A. M. J., 2007, Remote sensing applications to groundwater. IHPVI, Series on Groundwater No.16. United Nations Educational, Scientific and Cultural Organization.

Murthy, K.S.R., 2000, Groundwater potential in a semi-arid region of Andhra Pradesh: A Geographical information system approach. International Journal of Remote Sensing 21(9),1867–1884.

Maillet, R., 1947, Fundamentals equations of electrical prospecting. Geophysics (12) 529-556.

Nampak, H., Pradhan, B. and Manap, M.A., 2014, Application of GIS based data driven evidential Belief Function model to predict groundwater potential zonation. Journal of Hydrology. 513, 283–300.

Nwajide, C. S., 2013, Geology of Nigeria's Sedimentary Basins. CSS Bookshops Ltd, Lagos, Nigeria, 565.

Nabighian, M.N., 1984, Toward a Three-dimensional-Automatic Interpretation of Potential Field Data via Hilbert

transforms – Fundamental Relations. Geophysics, 49, 780-786.

Offodile, M.E., 2014, An Approach to Groundwater Studies in Nigeria; Mecon Geology and Engineering Services Limited: Jos, Nigeria.

Offodile, M.E., 1983, The Occurrence and exploitation of groundwater in Nigerian Basement Complex. Journal of Mining and Geology. 20. (3), 131-146.

Obaje, N. G., 2009, Geology and Mineral Resources of Nigeria. Published by Springer Dordtecht Heidelberg London, P. 218.

Olasehinde, P.I., 1999, An integrated geologic and geophysical exploration technique for Groundwater in the Basement Complex of West Central Nigeria. Water Res. J., 10, 46–49.

Pradhan, B., 2009, Groundwater potential zonation for basaltic watersheds using satellite Remote Sensing data and GIS techniques. Cent Eur J Geoscience 1, 120–129.

Prasad, R.K., Mondal, N.C., Banerjee P., Nandakumar, M. V. and Singh V. S. 2007, Deciphering Potential groundwater zone in hard rock through the application of GIS. Environmental Geology 55(3), 467–475.

Razandi, Y., Pourghasemi, H.R., Neisani, N.S. and Rahmati, O., 2015, Application of analytical Hierarchy Process, frequency ratio, and certainty factor models for groundwater potential mapping using GIS. Earth Sci Inf 8(4), 867–883.

Roest, W. R., Verhoef, J. and Pilkington, M., 1992, Magnetic interpretation using the 3-D analytic Signal. Geophysics, 57(1), 116–125. doi:10.1190/1.1443174.

Senthil Kumar, G.R. and Shankar, K., 2014, Assessment of groundwater potential zones using GIS. Frontiers in. Geosciences 2, 1–10.

Sreedher, G., Vijaya kumar, G.I., Murali Khrishna, I.V., Ercan, K. and Cuneyd, D.M., 2009, Mapping of groundwater potential zones in the Musi basin using remote sensing data and GIS. Advances in engineering software 40, 506 – 518.

Sultan, M., Wagdy, A., Manocha, N., Sauk, W., Abdel Gelil, K., Youssef, F., Becker, R., Milewski, A., El Alfy, Z. and Jones, C., 2008, An integrated approach for identifying aquifers in transcurrent fault systems: the Najd shear system of the Arabian Nubian shield. Journal of hydrology. 349, 475 – 488.

Sener, E., Davraz, A. and Ozcelik, M., 2005, An integration of GIS and remote sensing in Groundwater Investigations: a case study in Burdur, Turkey. Hydrogeology Journal 13, 826–834.

Sikdar, P.K., Chakraboty, S., Enakshi, A. and Paul, P.K., 2004, Land use/ Land cover changes And groundwater potential zoning in and around Raniganj coal mining area. Bardhaman district, west Bengal-GIS and remote sensing approach. Journal of Spatial hydrology.4, 1 – 24.

Shaban, A., Khawlie, M. and Abdallah, C., 2005, Use of remote sensing and GIS to determine Recharge potential zones: the case of occidental Lebanon. Hydrogeology Journal. 14, 433–443.

Silverman, B. W., 1986, Density Estimation for Statistics and Data Analysis, Chapman & Hall, London.

Tahir, A.G., Garba, M.L. and Hassan, C., 2015, Lineaments Analysis to identify favorable Areas for Groundwater in Kano City, Northwestern Nigeria. Journal of Environment and Earth Science. 5(2).

Tukur, A., Samaila, N. K., Grimes, S. T., Kariya, I. I. and Chaanda, M. S., 2015, Two members Sub-division of the Bima Sandstone, Upper Benue Trough: Based on sedimentological data. Journal of African Earth Sciences, 104, 140–158.

Talabi, A. O. and Tijani, M. N., 2011, Integrated remote sensing and GIS approach to Ground-Water Potential assessment in the basement terrain of Ekiti area south-western Nigeria. RMZ—Mater Geo-environment 58(3), 303–328.

Todd, K.D., 1980, Groundwater hydrology. Third edition. John Wiley and sons, New York, P. 636.

Yusuf, A., Olasehinde, A., Mboringong, M.N., Tabale, R.P. and Daniel, E.P., 2018, Evaluation Of Heavy metals concentration in groundwater around Kashere and its environs, Upper Benue trough, Northeastern Nigeria. Global Journal of Geological Sciences. 16, 25-36.

Zaborski, P.M.P., Ugodulunwa, F., Idorningie A., Nnabo, P. and Ibe, K., 1997, Stratigraphy and Structure of the

cretaceous Gongola Basin, Northeastern Nigeria. Bulletin in centres research exploration- production Elf- Aquitaine 21, 153-185.

Appendix (A)

Computed geo-electric parameters, inferred the lithology and the identified aquifer system

VES NO & LOCATION	CO-ORDINATE & ELEVATION	LAYER NO	APPARENT RESISTIVITY(Ω/m)	THICKNESS (m)	INFERED LITHOLOGY	CURVE TYPE	AQUIFER SYSTEM
VES 01 Pantami	N10^{0}16'05" E11^{0}10'27" Alt. 431m	1	25.4	1.6	Clayey topsoil	HKH	Fine grain Sand
		2	0.6	7.5	Clayey sand		
		3	52.6	18.6	Medium grained Sand		
		4	30.3	21.4	Fine grained Sand		
		5	39.8	---	Fine grained Sandy clay		
VES 02 G R A Gombe	N10^{0}16'30" E11^{0}08'28" Alt. 527m	1	32.7	1.6	Clayey topsoil	KHA	Silty sand
		2	59.2	35.2	Fine sands		
		3	51.2	53.1	Shale & mudstone.		
		4	86.9	45.5	Silty sand		
		5	96.6	---	Silty shale		
VES 03 Near FCE Gombe	N10^{0}19'16" E11^{0}09'47" Alt. 472m	1	45.1	1.8	Lateritic sand topsoil	KHK	Medium grained sand
		2	114.1	16.1	Coarse sand		
		3	34.6	57.3	Medium grain sand		
		4	76.9	64.6	Fine grained sandy clay		
		5	70.7	---	Clay		
VES 04 Malam Inna Gombe	N10^{0}18'28" E11^{0}10'48" Alt. 433m	1	35.5	3.2	Sandy topsoil	HKH	Fine grained Sand
		2	10.0	7.4	Clayey sand		
		3	147.1	41.9	Coarse grained Sand		
		4	59.2	22.0	Fine grained Sand		
		5	77.3	---	Medium grained clayey Sand		
VES 05 Opp. Govt. House Gombe	N10^{0}17'11" E11^{0}09'50" Alt. 455m	1	17.4	1.9	topsoil	HKH	Medium grained sand
		2	7.3	17.3	Clayey sands		
		3	109.9	42.3	Ironstone & mudstone.		
		4	47.1	24.0	Medium grained sand		
		5	64.7	---	Silty shale		
VES 06 Dawo Gadam	N10^{0}33'42" E11^{0}06'59" Alt. 409m	1	416.8	4.2	Dry sandy topsoil	HKH	Whitish grey Siltstones
		2	128.7	31.8	Clayey sand		
		3	241.1	44.3	Coarse grey sandstones		
		4	180.8	33.8	Whitish grey Siltstones		
		5	188.2	---	Clayey-Silts		
VES 07 Malam Sidi	N10^{0}27'57" E11^{0}17'29" Alt. 312m	1	114.7	2.0	Sandy topsoil	HK	Medium grained sandy clay.
		2	71.2	22.7	Medium grained sandy clay.		
		3	109.3	22.5	Coarse grained Sandy clay		
		4	95.8	---	Medium grained sandy Silt		
VES 08 Gwiwa Nayi Nawa	N10^{0}32'32" E11^{0}18'16" Alt. 332m	1	92.9	3.7	Sandy topsoil	HK	Medium-fine grained sandstone
		2	44.7	26.2	Sandy Shale		
		3	113.3	37.9	Medium-fine grained sandstones		
		4	89.8	---	Sandy clay		
VES 09 Salmanu Daban Fulani	N10^{0}24'19" E11^{0}21'55" Alt. 333m	1	63.4	1.1	Topsoil	HKH	Medium grained sandstone
		2	15.9	10.4	Clayey sand		
		3	110.6	35.6	Siltstones		
		4	53.9	19.1	Medium grained sandstones		
		5	79.4	---	Silty Shale		
VES 10 Tongo	N10^{0}51'10" E11^{0}26'14" Alt. 292m	1	84.8	4.6	Sandy topsoil	HK	Coarse grained Sand
		2	11.9	15.1	Coarse grained Sand		
		3	121.5	47.5	Clayey sand		
		4	39.8	---	Shale		
VES 11 Bajoga	N10^{0}27'57" E11^{0}17'29" Alt. 312m	1	45.6	2.9	Clayey Topsoil	HKH	Medium-grained Sand
		2	15.9	10.0	Sandy Shale		
		3	158.5	29.1	Mudstones/ ironstones		
		4	83.0	19.8	Medium-grained sandstones		
		5	105.4	---	Sandy clay		
VES 12 Jalingo Ashaka	N10^{0}55'12" E11^{0}28'25" Alt. 310m	1	88.8	5.5	Sandy topsoil	HKH	Medium grained Sandy Limestone
		2	16.1	14.6	Clayey sand		
		3	94.2	17.3	Medium grained Sand, Limestone		
		4	71.0	10.4	Medium grained Sandy Limestone		
		5	146.7	---	Limestone		

Appendix (A)

VES NO & LOCATION	CO-ORDINATE & ELEVATION	LAYER NO	APPARENT RESISTIVITY(Ω/m)	THICKNESS (m)	INFERED LITHOLOGY	CURVE TYPE	AQUIFER SYSTEM
VES 13 Munda	N10^{0}48'59" E11^{0}19'04" Alt. 428m	1	110.9	5.9	Sandy topsoil	HK	Coarse grained sandstone
		2	52.9	30.6	Fine grained sandy clay, Dry Shale.		
		3	116.6	46.11	Coarse grained sandstone		
		4	93.9	---	Medium grained sandy Silt		
VES 14 Birin Fulani	N10^{0}53'42" E11^{0}16'10" Alt. 429m	1	18.3	1.2	Clayey Topsoil	HKH	Fine grained Sand
		2	5.9	4.3	Clayey sand		
		3	72.4	18.6	Medium grained sandy clay		
		4	44.2	19.4	Fine grained Sand		
		5	73.9	---	Greyish sandy clay		
VES 15 Barwo Nasarawo	N11^{0}06'01" E11^{0}14'35" Alt. 264m	1	24.7	5.5	Sandy topsoil	QQ	Clayey sand
		2	17.8	14.9	Grayish Clayey sand		
		3	12.5	9.7	Clayey sand		
		4	6.5	---	Clayey Shale		
VES 16 Guduku	N11^{0}05'20" E11^{0}09'19" Alt. 345m	1	129.9	6.8	Sandy topsoil	AKH	Fine Quartz sandstone
		2	149.8	12.0	Silty clay		
		3	344.4	34.1	Coarse Quartz sandstones		
		4	174.8	20.6	Fine Quartz sandstones		
		5	229.2	---	Medium Quartz sandstones		
VES 17 Jigawan Nafada	N11^{0}09'39" E11^{0}06'58" Alt. 432m	1	120.2	6.4	Lateritic sand topsoil	KQH	Fine Quartz sandstone
		2	238.2	22.3	Coarse sand		
		3	226.7	32.1	Medium Quartz sandstones		
		4	170.0	22.7	Fine Quartz sandstones		
		5	220.3	---	Medium Quartz sandstones		
VES 18 Tsamiyar Hutu	N11^{0}19'33" E11^{0}12'25" Alt. 451m	1	698.4	1.8	Dry lateritic sand topsoil	HKH	Coarse Quartz sandstone
		2	272.0	16.3	Medium Quartz sandstones		
		3	152.0	40.1	Coarse Quartz sandstones		
		4	578.2	34.9	medium grain Quartzo-felsparthic sandstones		
		5	824.5	---	Coarse Quartz sandstones		
VES 19 Gube	N11^{0}05'08" E11^{0}23'36" Alt. 273m	1	57.4	3.4	Sandy topsoil	HK	Medium grained sandstone
		2	10.5	11.3	Sandy shale		
		3	55.2	22.2	Medium grained sandstone		
		4	45.5	---	Claystone		
VES 20 Kalajanga	N10^{0}15'35" E11^{0}13'11" Alt. 414m	1	35.9	3.0	Clayey topsoil	HKH	Fine grained sandy clay
		2	10.5	11.1	Clayey sands		
		3	297.9	42.8	Coarse grained Sand, Ironstone& Mudstone.		
		4	69.3	16.4	Fine grained sandy clay		
		5	124.8	---	Coarse grained sandy clay		
VES 21 Kumo	N10^{0}03'01" E11^{0}12'38" Alt. 403m	1	25.8	2.3	Clayey topsoil	HKH	Medium grained sandstone
		2	7.5	5.0	Sandy Shale		
		3	94.2	17.9	Ironstone & Mudstone.		
		4	44.8	22.1	Medium grained sandstones		
		5	52.2	---	Sandy Clay		
VES 22 Baganje	N09^{0}51'09" E11^{0}10'27" Alt. 3437m	1	69.1	1.0	Sandy topsoil	HKH	Medium grained sandstone
		2	18.9	16.2	Sandy Clay		
		3	59.8	20.8	Ironstones/mudstones		
		4	53.7	21.4	Medium grained sandstones		
		5	70.0	---	Silty shale		

Appendix (A)

VES NO & LOCATION	CO-ORDINATE & ELEVATION	LAYER NO	APPARENT RESISTIVITY(Ω/m)	THICKNESS (m)	INFERED LITHOLOGY	CURVE TYPE	AQUIFER SYSTEM
VES 23 Tudu Kwaya	N09^{0}42'13" E11^{0}03'55" Alt. 344m	1	151.0	3.1	Sandy topsoil	QHA	Fine grained sandstone
		2	63.3	26.8	Fine grained sandstones		
		3	62.2	33.0	Fine grained sandstones		
		4	78.3	21.6	Medium grained sandstones		
		5	105.6	---	Medium - Coarse grained sandstones		
VES 24 Lalapido	N09^{0}43'22" E11^{0}08'52" Alt. 398m	1	125.2	9.0	Sandy topsoil	HA	Medium grained sandstone
		2	31.9	31.1	Sandy Shale		
		3	66.1	35.2	Medium grained sandstones		
		4	78.8	---	Claystones		
VES 25 Filiya	N09^{0}35'09" E11^{0}06'01" Alt. 390m	1	95.8	1.7	Sandy topsoil	HKH	Medium grained sandstone
		2	86.6	5.4	Clayey sands		
		3	485.0	43.1	Coarse grained sandstones		
		4	89.0	17.4	Medium grained sandstones		
		5	136.4	---	Medium - Coarse grained sandstones		
VES 26 Gundale	N09^{0}34'01" E11^{0}01'38" Alt. 360m	1	141.3	12.7	Sandy topsoil	HKH	Medium grained sandstone
		2	35.7	16.4	Clayey sands		
		3	142.4	41.7	Medium - Coarse grained sandstones		
		4	107.0	22.1	Medium grained sandstones		
		5	132.7	---	Medium – Coarse grained sandstones		
VES 27 Billiri	N09^{0}53'17" E11^{0}13'23" Alt. 444m	1	37.8	1.4	Clayey topsoil	KHA	Medium grained sandstone
		2	152.1	5.4	Sandy shale		
		3	38.2	32.1	Siltstones		
		4	64.7	22.2	Medium grained Sandstones		
		5	80.2	---	Claystones		
VES 28 Kaltungo	N09^{0}49'12" E11^{0}18'01" Alt. 499m	1	65.8	2.6	Sandy topsoil	HA	Weather. basement
		2	11.4	7.0	Clayey sands		
		3	80.0	37.5	Weathered basement		
		4	204.6	---	Fractured basement		
VES 29 Kulishin	N09^{0}48'29" E11^{0}16'35" Alt. 312m	1	78.0	4.2	Sandy topsoil	HA	Fractured basement
		2	39.3	25.3	Clayey sands		
		3	148.5	18.8	Fractured basement		
		4	488.6	---	Fresh basement		
VES 30 Kaltin	N09^{0}54'57" E11^{0}28'06" Alt. 325m	1	135.8	3.5	Sandy topsoil	HA	Fine grained sandstone
		2	19.4	52.1	Clayey sands		
		3	36.5	27.7	Fine grained sandstones		
		4	98.7	---	Medium grained sandstones		
VES 31 Cham	N09^{0}42'32" E11^{0}42'59" Alt. 418m	1	140.5	5.1	Sandy topsoil	HK	Medium grained Sand
		2	38.7	30.8	Clayey sand		
		3	75.2	37.9	Medium grained Sand		
		4	65.7	---	Medium grained Sandy silt		
VES 32 Shanwe Kulani	N09^{0}49'01" E11^{0}37'53" Alt. 561m	1	89.6	2.4	Sandy topsoil	HA	Medium-coarse grained sandstone
		2	14.4	30.7	Clayey sands		
		3	70.0	27.4	Medium-coarse grained sandstones		
		4	144.9	---	Medium - Coarse grained sandstones		
VES 33 Old Liji	N10^{0}19'14" E11^{0}14'04" Alt. 376m	1	15.2	3.6	Sandy topsoil	AK	Grayish colored sandstone
		2	30.9	23.1	Clayey sands		
		3	83.5	28.1	Grayish colored sandstones		
		4	81.7	---	Medium grained sandstones		
VES 34 Garin Baraya	N10^{0}12'27" E11^{0}18'43" Alt. 379m	1	128.4	7.6	Sandy topsoil	QH	Fine grained Sand
		2	44.2	30.9	Clayey sand		
		3	39.9	36.8	Fine grained Sand		
		4	58.0	---	Fine grained Sand clay		

Appendix (A)

VES NO & LOCATION	CO-ORDINATE & ELEVATION	LAYER NO	APPARENT RESISTIVITY(Ω/m)	THICKNESS (m)	INFERED LITHOLOGY	CURVE TYPE	AQUIFER SYSTEM
VES 35 Yaran – Dua Hinna	N10⁰21'18" E11⁰32'38" Alt. 266m	1	40.9	2.2	Reddish-brown topsoil	HA	Medium grained Sandston
		2	9.3	15.5	Clayey sand		
		3	67.9	23.6	Medium grained Sandstone		
		4	89.0	---	Silty shale		
VES 36 Garin Koshi	N10⁰31'36" E11⁰35'29" Alt. 317m	1	68.8	11.5	Topsoil	HA	Medium grained sandstone
		2	26.5	38.7	Clayey sand		
		3	40.5	29.6	Medium grained sandstones		
		4	58.3	---	Claystones		
VES 37 Dake Jara Gwal	N10⁰18'29" E11⁰35'14" Alt. 202m	1	59.2	2.8	Sandy topsoil	HKH	Medium grained sandstone
		2	16.0	6.3	Clayey sand		
		3	92.7	14.9	Siltstone		
		4	48.3	32.9	Medium grained sandstones		
		5	53.3	---	Silty shale		
VES 38 Dali Jara	N10⁰15'09" E11⁰41'52" Alt. 261m	1	95.4	1.4	Sandy topsoil	HA	Clayey sand
		2	19.3	25.4	Clayey sand		
		3	157.1	25.6	Medium grained sandstones		
		4	248.8	---	Silty shale		
VES 39 Balbiya	N10⁰37'16" E11⁰43'51" Alt. 265m	1	57.5	1.5	Sandy topsoil	HKH	Fine-medium grained sandstone
		2	14.2	5.2	Clayey sand		
		3	50.0	26.1	Siltstones		
		4	44.1	24.4	Fine-medium grained sandstones		
		5	111.8	---	Silty shale		
VES 40 Barmari	N11⁰04'32" E11⁰39'25" Alt. 314m	1	19.3	11.4	Clayey topsoil	AA	Medium grained sandstone
		2	35.4	19.0	Clayey sand		
		3	85.2	28.1	Medium grained Sandstones		
		4	95.8	---	Claystones		
VES 41 Kashere	N09⁰54'19" E11⁰0.4'05" Alt. 351m	1	123.9	3.3	Sandy topsoil	HA	Coarse grained sandy Silt
		2	29.4	18.1	Fine grained clayey sand		
		3	141.6	25.8	Coarse grained sandy Silt		
		4	143.4	---	Coarse grained sandy Silt/ironstone		
VES 42 Barambu	N10⁰07'07" E10⁰42'43" Alt. 318m	1	269.5	9.8	Sandy topsoil	QH	Medium grain Sands.
		2	112.8	42.8	Medium grain Sandstone		
		3	103.9	32.0	sandy clay		
		4	107.5	---	Silty shale		
VES 43 Futuk	N09⁰50'16" E10⁰54'01" Alt. 392m	1	87.1	5.8	Sandy topsoil	HA	Silty sand
		2	18.2	41.3	Clayey silt		
		3	53.8	33.1	Silty sand		
		4	79.0	---	Fine Quartz sandstones		
VES 44 Digare	N09⁰39'29" E10⁰44'60" Alt. 312m	1	93.7	6.0	Sandy topsoil	HK	Clayey silt
		2	9.3	12.2	Clayey silt		
		3	170.2	52.6	Medium Quartz sandstones		
		4	83.1	---	Fine Quartz sandstones		
VES 45 Kwakwaladi	N10⁰15'28" E10⁰15'27" Alt. 465m	1	26.0	1.4	Clayey topsoil	AA	Weather. basement
		2	99.1	24.3	Weathered basement		
		3	441.0	20.5	Fractured basement		
		4	982.8	---	Fresh basement		
VES 46 Wuro Dole	N10⁰20'32" E10⁰49'32" Alt. 358m	1	438.7	8.2	Lateritic sand topsoil	HKH	Fine Quartz sandstone
		2	147.1	31.1	Coarse sand		
		3	390.6	28.1	Medium Quartz sandstones		
		4	232.8	33.1	Fine Quartz sandstones		
		5	280.0	---	Medium Quartz sandstones		
VES 47 Duggal Zange	N10⁰35'22" E10⁰46'22" Alt. 400m	1	141.1	3.0	Sandy topsoil	HKH	Whitish grey sandstone
		2	61.2	8.7	Clayey grey sand		
		3	742.1	25.4	Coarse grey Sand		
		4	354.4	18.4	Whitish grey sandstones		
		5	493.1	---	Whitish grey sandy clay		

Appendix (A)

VES NO & LOCATION	CO-ORDINATE & ELEVATION	LAYER NO	APPARENT RESISTIVITY(Ω/m)	THICKNESS (m)	INFERED LITHOLOGY	CURVE TYPE	AQUIFER SYSTEM
VES 48 Galdo	N10^{0}59'29" E10^{0}48'01" Alt. 356m	1	205.3	2.0	Sandy topsoil	HA	Fine grained grey sand
		2	74.1	25.5	Sandy clay		
		3	151.5	17.6	Fine grained grey sand		
		4	252.9	---	Coarse grained grey sand		
VES 49 Garin Bauchi	N11^{0}01'14" E10^{0}47'02" Alt. 335m	1	76.6	3.1	Sandy topsoil	HK	Clayey sand
		2	26.9	12.7	Clayey sand		
		3	179.6	29.8	Medium grained kaolinated sand		
		4	125.0	---	Medium grained kaolinated sand/mudstones		
VES 50 Walowa Maube	N10^{0}42'28" E10^{0}34'03" Alt. 398m	1	725.9	5.3	Sandy topsoil	HK	Coarse grained grey sand
		2	80.6	17.6	Sandy clay		
		3	424.9	51.7	Coarse grained grey sand		
		4	183.2	---	Fine grained grey sand		
VES 51 Darazo	N10^{0}59'44" E10^{0}24'22" Alt. 510m	1	84.9	3.9	Sandy topsoil	HA	Medium grained sand
		2	31.7	33.9	Clayey sand		
		3	49.4	43.2	Medium grained sand		
		4	54.4	---	Fine grained kaolinated sand		
VES 52 Misau	N11^{0}18'09" E10^{0}27'46" Alt. 443m	1	85.3	2.4	Sandy topsoil	HA	Weathered basement
		2	23.9	6.4	Clayey sands		
		3	79.0	32.8	Weathered basement		
		4	360.7	---	Fractured basement		
VES 53 Giade	N11^{0}23'08" E10^{0}12'17" Alt. 468m	1	108.5	2.9	Sandy topsoil	HA	weathered basement
		2	36.5	24.9	Clayey sands		
		3	132.9	32.3	weathered basement		
		4	163.7	---	Fractured basement		
VES 54 Jigawan Yamu	N10^{0}12'59" E11^{0}31'30" Alt. 289m	1	45.4	4.2	Clay topsoil	HA	Fine grained Sand
		2	33.9	30.0	Clayey sand		
		3	54.9	25.8	Fine grained Sand		
		4	77.0	---	Medium grained Sand		
VES 55 Tallase	N09^{0}58'09" E11^{0}40'43" Alt. 295m	1	50.0	7.9	Sandy topsoil	HKH	Fine grained sandstones
		2	10.2	11.0	Clayey sand		
		3	60.5	29.3	Fine grained sandstones		
		4	30.2	42.0	Fine grained sandstones		
		5	30.8	---	Fine grained sandstones		
VES 56 Guyuk	N09^{0}54'42" E11^{0}57'15" Alt. 196m	1	71.8	5.3	Sandy topsoil	QQ	Fine grained Sand
		2	56.1	30.5	Fine grained sandy clay		
		3	17.6	31.9	Fine grained Sand		
		4	13.5	---	Clayey shale		
VES 57 Lakundum	N10^{0}10'54" E11^{0}57'29" Alt. 264m	1	75.5	1.8	Sandy topsoil	HA	Weathered basement
		2	15.7	2.5	Clayey sands		
		3	73.9	42.7	Weathered basement		
		4	501.2	---	Fractured basement		
VES 58 Kubuku	N10^{0}25'29" E11^{0}55'44" Alt. 293m	1	167.1	1.2	Sandy topsoil	KQ	Medium - Coarse grained sandstone
		2	502.9	15.5	Coarse grained sandstones		
		3	215.5	35.0	Medium - Coarse grained sandstones		
		4	189.0	---	Medium - fine grained sandstones		
VES 59 Kwaya Kusar	N10^{0}29'58" E11^{0}50'30" Alt. 411m	1	37.4	1.7	Clayey topsoil	HA	Weathered basement
		2	18.0	5.5	Clayey sands		
		3	84.3	37.2	Weathered basement		
		4	120.3	---	Fractured basement		
VES 60 Wuyo	N10^{0}23'07" E11^{0}41'41" Alt. 308m	1	78.3	5.8	Sandy topsoil	QH	Fine grained sandstone
		2	39.9	30.5	medium grained clayey sand		
		3	29.6	45.0	Fine grained sandstones		
		4	33.3	-	Medium - Fine grained sandstones		

Appendix (B)

Computed Dar-zarouk (hydraulic) parameters for the study area.

VES No	Locations	Layer Resistivity (ohm-m)	Layer Thickness (m)	Aquifer Conductivity	Longitudinal Conductance	Transverse Resistance	Hydraulic Conductivity (m/day)	Transmisivity (m²/day)
1	PANTAMI	30.3	21.4	0.0330033	0.706270627	648.42	16.03625637	343.1758863
2	GRA GOMBE	86.9	45.5	0.01150748	0.523590334	3953.95	6.00152058	273.0691864
3	NEAR FCE GOMBE	65.5	64.6	0.015267176	0.986259542	4231.3	7.812548849	504.6906557
4	MALAM INNA GOMBE	59.2	22	0.016891892	0.371621622	1302.4	8.585434121	188.8795507
5	OPP. GOVT. HOUSE GOMBE	28.1	30	0.035587189	1.067615658	843	17.20443447	516.133034
6	DAWO GADAM	180.8	33.8	0.005530973	0.186946903	6111.04	3.030084291	102.416849
7	MALAM SIDI	71.2	22.7	0.014044944	0.318820225	1616.24	7.227501746	164.0642896
8	GWIWA NAYI NAWA	44.7	26.2	0.022371365	0.586129754	1171.14	11.15785597	292.3358263
9	SALMANU DABAN FULANI	53.9	19.1	0.018552876	0.354359926	1029.49	9.370422431	178.9750684
10	TONGO	11.9	15.1	0.084033613	1.268907563	179.69	38.34728717	579.0440362
11	BAJOGA	83	19.8	0.012048193	0.238554217	1643.4	6.264169503	124.0305562
12	JALINGO ASHAKA	71	10.4	0.014084507	0.146478873	738.4	7.246491587	75.3635125
13	MUNDA	116.6	46.1	0.008576329	0.395368782	5375.26	4.562036009	210.30986
14	BIRIN FULANI	44.2	19.4	0.022624434	0.438914027	857.48	11.2755533	218.745734
15	BARWO NASSARAWO	12.5	14.5	0.08	1.16	181.25	36.62743871	531.0978613
16	GUDUKU	174	20.6	0.005747126	0.118390805	3584.4	3.140404294	64.69232845
17	JIGAWA NAFADA	170	22.7	0.005882353	0.133529412	3859	3.209278823	72.85062929
18	TSAMIYAR HUTU	152	40.1	0.006578947	0.263815789	6095.2	3.562443323	142.8539772
19	GUBE	55.2	22.2	0.018115942	0.402173913	1225.44	9.164401081	203.449704
20	KALAJANGA	28.3	29.4	0.035335689	1.038869258	832.02	17.09098831	502.4750563
21	KUMO	44.8	22.8	0.022321429	0.508928571	1021.44	11.13462123	253.869364
22	BAGANJE	53.7	21.4	0.018621974	0.398510242	1149.18	9.402973341	201.2236295
23	TUDU KWAYA	38.5	39.5	0.025974026	1.025974026	1520.75	12.82542559	506.6043109
24	LAILAPIDO	66.1	35.2	0.015128593	0.532526475	2326.72	7.746376303	272.6724459
25	FILIYA	89	17.4	0.011235955	0.195505618	1548.6	5.869317967	102.1261326
26	GUNDALE	107	22.1	0.009345794	0.206542056	2364.7	4.942731832	109.2343735
27	BILLIRI	38.2	32.1	0.02617801	0.840314136	1226.22	12.91935854	414.711409
28	KALTUNGO	80	37.5	0.0125	0.46875	3000	6.483024833	243.1134312
29	KULISHIN	148.5	18.8	0.006734007	0.126599327	2791.8	3.640705333	68.44526026
30	KALTIN	36.5	27.7	0.02739726	0.75890411	1011.05	13.47980051	373.3904741
31	CHAM	75.2	37.9	0.013297872	0.503989362	2850.08	6.868229989	260.3059166
32	SHANWE KULANI	70	27.4	0.014285714	0.391428571	1918	7.34301327	201.1985636
33	OLD LIJI	83.5	28.1	0.011976048	0.336526946	2346.35	6.229172	175.0397332
34	GARIN BARAYA	39.9	36.8	0.025062657	0.922305764	1468.32	12.40513719	456.5090485
35	YARAN DUA HINNA	9.3	15.5	0.107526882	1.666666667	144.15	48.26220598	748.0641927
36	GARIN KOSHI	40.5	29.6	0.024691358	0.730864198	1198.8	12.23361612	362.115037
37	DAKE JARA GWAL	48.3	32.9	0.020703934	0.68115942	1589.07	10.38008036	341.5046439
38	DAKE JARA	19.3	25.4	0.051813472	1.316062176	490.22	24.42478183	620.3894585
39	BALBIYA	44.1	24.4	0.022675737	0.553287982	1076.04	11.29940222	275.7054142
40	BARMARI	85.2	28.1	0.011737089	0.329812207	2394.12	6.113151383	171.7795539
41	KASHERE	141.6	25.8	0.007062147	0.18220339	3653.28	3.805929884	98.19299101
42	BARAMBU	112.8	42.8	0.008865248	0.379432624	4827.84	4.705238266	201.3841978
43	FUTUK	53.8	33.1	0.018587361	0.615241636	1780.78	9.38666865	310.6987323
44	DIGARE	9.3	12.2	0.107526882	1.31827957	113.46	48.26220598	588.7989129
45	KWAKWALA	99.1	24.3	0.010090817	0.245206862	2408.13	5.309330134	129.0167223
46	WURO DOLE	232.8	33.1	0.004295533	0.142182131	7705.68	2.393560384	79.22684872
47	DUGGAL ZANGE	354.4	18.4	0.00282167	0.051918736	6520.96	1.617308605	29.75847833
48	GALDO	151.5	17.6	0.00660066	0.116171617	2666.4	3.573409614	62.8920092
49	GARIN BAUCHI	26.9	12.7	0.037174721	0.472118959	341.63	17.91931065	227.5752452
50	WALOWA MAUBE	424.9	51.7	0.002353495	0.121675688	21967.33	1.365502207	70.5964641
51	DARAZO	49.4	43.2	0.020242915	0.874493927	2134.08	10.1643078	439.0980969
52	MISAU	79	32.8	0.012658228	0.415189873	2591.2	6.559543828	215.1530376
53	GIADE	132.9	32.3	0.007524454	0.24303988	4292.67	4.037841895	130.4222932
54	JIGAWAN YAMU	54.9	25.8	0.018214936	0.469945355	1416.42	9.211107433	237.6465718
55	TALLASE	30.2	42	0.033112583	1.390728477	1268.4	16.08578431	675.6029411
56	GUYUK	17.6	31.9	0.056818182	1.8125	561.44	26.61861996	849.1339768
57	LAKUNDUM	73.9	42.7	0.0135318	0.577807848	3155.53	6.98086961	298.0831324
58	KUBUKU	215.5	35	0.004640371	0.162412993	7542.5	2.572334821	90.03171873
59	KWAYA KUSAR	84.3	37.2	0.011862396	0.441281139	3135.96	6.17401075	229.6731999
60	WUYO	29.6	45	0.033783784	1.52027027	1332	16.38974026	737.5383115
	Minimum:	**9.3**	**12.7**	**0.002353495**	**0.051918736**	**113.46**	**1.365502207**	**29.75847833**
	Maximum:	**424.9**	**64.6**	**0.107526882**	**1.81250000**	**21967.33**	**48.26220598**	**849.1339768**
	Average:	**85.52200**	**29.0966667**	**0.002271267**	**0.5791154**	**2638.83033**	**11.06753836**	**285.7863313**

Appendix (C)

The aquifer transmisivity values classified after Offodile (1983).

VES No	Locations	Transmisivity	Aquifer potentials
1	PANTAMI	343.1758863	Moderate potentials
2	GRA GOMBE	273.0691864	Moderate potentials
3	NEAR FCE GOMBE	504.6906557	High potentials
4	MALAM INNA GOMBE	188.8795507	Moderate potentials
5	OPP. GOVT. HOUSE GOMBE	516.133034	High potentials
6	DAWO GADAM	102.416849	Moderate potentials
7	MALAM SIDI	164.0642896	Moderate potentials
8	GWIWA NAYI NAWA	292.3358263	Moderate potentials
9	SALMANU DABAN FULANI	178.9750684	Moderate potentials
10	TONGO	579.0440362	High Potentials
11	BAJOGA	124.0305562	Moderate potentials
12	JALINGO ASHAKA	75.3635125	Moderate potentials
13	MUNDA	210.30986	Moderate potentials
14	BIRIN FULANI	218.745734	Moderate potentials
15	BARWO NASSARAWO	531.0978613	High potentials
16	GUDUKU	64.69232845	Moderate potentials
17	JIGAWAN NAFADA	72.85062929	Moderate potentials
18	TSAMIYAR HUTU	142.8539772	Moderate potentials
19	GUBE	203.449704	Moderate potentials
20	KALAJANGA	502.4750563	High potentials
21	KUMO	253.869364	Moderate potentials
22	BAGANJE	513.021265	High potentials
23	TUDU KWAYA	506.6043109	High potentials
24	LAILAPIDO	272.6724459	Moderate potentials
25	FILIYA	102.1261326	Moderate potentials
26	GUNDALE	109.2343735	Moderate potentials
27	BILLIRI	414.711409	Moderate potentials
28	KALTUNGO	243.1134312	Moderate potentials
29	KULISHIN	68.44526026	Moderate potentials
30	KALTIN	373.3904741	Moderate potentials
31	CHAM	260.3059166	Moderate potentials
32	SHANWE KULANI	201.1985636	Moderate potentials
33	OLD LIJI	175.0397332	Moderate potentials
34	GARIN BARAYA	456.5090485	Moderate potentials
35	YARAN DUA HINNA	748.0641927	High Potentials
36	GARIN KOSHI	362.115037	Moderate potentials
37	DAKE JARA GWAL	341.5046439	Moderate potentials
38	DAKE JARA	620.3894585	High Potentials
39	BALBIYA	275.7054142	Moderate potentials
40	BARMARI	171.7795539	Moderate potentials
41	KASHERE	98.19299101	Moderate potentials
42	BARAMBU	201.3841978	Moderate potentials
43	FUTUK	310.6987323	Moderate potentials
44	DIGARE	588.7989129	High Potentials
45	KWAKWALA	129.0167223	Moderate potentials
46	WURO DOLE	79.22684872	Moderate potentials
47	DUGGAL ZANGE	29.75847833	Moderate potentials
48	GALDO	62.8920092	Moderate potentials
49	GARIN BAUCHI	227.5752452	Moderate potentials
50	WALOWA MAUBE	70.5964641	Moderate potentials
51	DARAZO	439.0980969	Moderate potentials
52	MISAU	215.1530376	Moderate potentials
53	GIADE	130.4222932	Moderate potentials
54	JIGAWAN YAMU	237.6465718	Moderate potentials
55	TALLASE	675.6029411	High Potentials
56	GUYUK	849.1339768	High Potentials
57	LAKUNDUM	298.0831324	Moderate potentials
58	KUBUKU	90.03171873	Moderate potentials
59	KWAYA KUSAR	229.6731999	Moderate potentials
60	WUYO	737.5383115	High Potentials

Appendix (D)

Bore yields measurements across the study area.

S/NO	location/ coordinates	Borehole depth (m)	Static water Table (m)	draw down (m)	discharge (l/s)	Yield (l/min)	REMARKS
1	Dayayi Makabarta N10^{0}54'27" E11^{0}28'37" Alt: 289m	44	8.87	11.41	1.0	60	Very High Yield
2	Juggol Fulani N10^{0}57'23" E11^{0}30'01" Alt: 269m	44	3.74	12.99	1.056	63.38	Very High Yield
3	G.J.S.S.Bage N10^{0}56'46'' E11^{0}22'54'' Alt. 310m	50	3.9	2.8	1.1	67	Very High Yield
4	Bajoga N10^{0}51'11" E11^{0}26'14" Alt. 292m	58	26.73	4.47	0.9036	54.22	High Yield
5	PHC Birin Bolewa N10^{0}54'09.3'' E11^{0}16'06.5'' Alt. 441m	45	25.64	0.14	1.3	78.26	Very High Yield
6	PHC Birin-Fulani N10^{0}53'42" E11^{0}16'10" Alt. 429m	40	22.64	0.17	1.36	81.81	Very High Yield
7	Guduku, N11^{0}05'20" E11^{0}09'19" Alt. 345m	64	3.4	2.52	1.25	75	Very High Yield
8	Dogon Kawo N10^{0}8'13'' E11^{0}35'25'' Alt. 281m	138	50	25.43	1.0	60	Very High Yield
9	Garin Koshi N10^{0}31'36" E11^{0}35'29" Alt. 317m	60	17	1.89	1.0	60	Very High Yield
10	Biryel N10^{0}21'07'' E11^{0}36'23'' Alt. 243m	60	8.66	1.92	1.56	93.75	Very High Yield
11	Phc Garin Gado N10^{0}29'19'' E11^{0}39'44'' Alt. 347m	40	4.2	13.82	1.4	83	Very High Yield
12	Kurba Gayi N10^{0}28'23'' E11^{0}46'32'' Alt. 339m	65	1.1	35.3	1.3	78	Very High Yield
13	Wuyo. N10^{0}23'02'' E11^{0}41'36'' Alt. 309m	50.9	2.4	13.03	1.21	72.72	Very High Yield
14	Balbiya N10^{0}37'16" E11^{0}43'51" Alt. 265m	68	0.3	16.21	1.26	75.34	Very High Yield
15	Reme Primary School N09^{0}54'11" E11^{0}39'21" Alt: 396m	60	16.85	4.22	1.14	68.18	Very High Yield
16	G.J.S.S. Bambam N9^{0}41'18'' E11^{0}32'19'' Alt. 251m	60	5.5	7.7	1	60	Very High Yield
17	G.J.S.S. Kaltungo N9^{0}51'12'' E11^{0}24'32'' Alt. 377m	50	6.4	1.9	1.2	72	Very High Yield

Appendix (D)

S/NO	location/ coordinates	Borehole depth (m)	Static water Table (m)	draw down (m)	discharge (l/s)	Yield (l/min)	REMARKS
18	PHC Kalarin N09^{0}48'37.84'' E11^{0}18'41.62'' Alt. 510m	32	5.61	3.29	1.47	88.24	Very High Yield
19	G.J.S.S Sabon Wange N9^{0}51'12'' E11^{0}24'32'' Alt. 377m	70	1.1	7.1	1.33	80	Very High Yield
20	G.J.S.S Gandu N10^{0}17'48'' E11^{0}10'28' Alt. 441m	84	50	25.43	1	60	Very High Yield
21	Hurumin Dau N10^{0}16'19'' E11^{0}10'46'' Alt: 419m	65	23.5	5.47	1.03	61.62	Very High Yield
22	Bolari Near Audu Rice N10^{0}18'39'' E11^{0}10'30'' Alt. 465m	59	15	13.46	1.2	71	Very High Yield
23	Kwakwaladi N10^{0}15'28'' E10^{0}15'27'' Alt. 465m	55	26.89	2.38	1.19	71.43	Very High Yield
24	Sabon Gari N11^{0}12'28'' E10^{0}50'23'' Alt. 354m	66	3.9	2.8	1.06	64	Very High Yield
25	Bajoga N10^{0}51'11'' E11^{0}26'14'' Alt. 292m	58	26.73	4.47	0.9036	54.22	High Yield
26	G.J.S.S Barwo Nasarawo N11^{0}5'58'' E11^{0}14'31'' Alt. 285m	30	4.2	13.82	0.9	55	High Yield
27	Ngalda N11^{0}06'46'' E11^{0}22'29'' Alt. 276m	31	4.92	6.77	0.88	52.94	High Yield
28	Katsira N11^{0}07'20'' E10^{0}56'08'' Alt: 300m	50	20.02	0.78	0.852	51.136	High Yield
29	Galdo N10^{0}59'29'' E10^{0}48'01'' Alt: 356m	46.3	13.33	0.71	0.857	51.43	High Yield
30	Jigawan Yamu N10^{0}12'59'' E11^{0}31'30'' Alt. 298m	43	9.0	11.11	0.833	50	High Yield
31	Barmari Gabai N11^{0}04'32'' E11^{0}39'25'' Alt. 314m	65	54.72	2.7	0.93	55.56	High Yield
32	Lawanti Gabai N11^{0}04'27'' E11^{0}39'27'' Alt.295m	60	17	1.89	0.893	53.57	High Yield
33	Malam Bukarti N11^{0}04'32'' E11^{0}39'30'' Alt. 306m	65	15	13.46	0.914	54.88	High Yield
34	Gadina Pri. Sch N11^{0}04'32'' E11^{0}39'21'' Alt. 295m	60	16	7.2	0.833	50	High Yield

Appendix (D)

S/NO	location/ coordinates	Borehole depth (m)	Static water Table (m)	draw down (m)	discharge (l/s)	Yield (l/min)	REMARKS
35	Dumbulwa N11^{0}07'47'' E11^{0}28'13'' Alt. 289m	60	2.4	13.03	1.25	75	Very High Yield
36	PHC Guwal N10^{0}32'30'' E11^{0}54'44'' Alt. 462m	48	12	12.41	0.97	50.06	High Yield
37	PHC Kubuku N10^{0}25'29'' E11^{0}55'44'' Alt. 365m	50	15	13.46	0.87	52.17	High Yield
38	PHC K/Kusar N10^{0}29'58'' E11^{0}50'30'' Alt. 411m	50	15	13.33	0.87	52.17	High Yield
39	Yimirdlang N10^{0}23'31'' E11^{0}50'55'' Alt. 283m	62	12	12.41	0.91	55.OO	High Yield
40	Guyuk N9^{0}54'47'' E11^{0}57'17'' Alt. 198m	60	26.1	3.08	0.95	56.96	High Yield
41	Kulani N09^{0}48'56'' E11^{0}37'47'' Alt. 580m	145	7.1	19.72	0.896	53.73	High Yield
42	Tula Wange N9^{0}50'40'' E11^{0}28'39'' Alt. 655m	120	54.72	2.7	0.89	54	High Yield
43	Tudu Kwaya N09^{0}42'13" E11^{0}03'55" Alt. 344m	60	13.9	8.4	0.94	56.6	High Yield
44	Galdimari N10.125358 E11.129371 Alt: 446m	36	1.26	16.83	0.93	56	High Yield
45	Shamaki N10^{0}17'53'' E11^{0}9'59'' Alt. 408m	55	40.6	0.71	0.83	50	High Yield
46	Wailo N10^{0}40'19'' E10^{0}12'48'' Alt. 515m	45	1.1	7.1	0.85	51.06	High Yield
47	Misau N11^{0}18'09" E10^{0}27'46" Alt. 443m	55	28.61	3.14	0.99	59.21	High Yield
48	Sabon Sara N11^{0}25'56'' E10^{0}18'08'' Alt. 442m	55	28.29	16.8	0.99	56.96	High Yield
49	Mabani N10^{0}54'12" E11^{0}21'12" Alt. 340m	41	14.37	16.53	0.824	49.45	Moderate Yield
50	Garin Alarrama N11^{0}17'01'' E10^{0}58'35'' Alt. 380m	130	80	47.62	0.69	42.93	Moderate Yield

Appendix (D)

S/NO	location/ coordinates	Borehole depth (m)	Static water Table (m)	draw down (m)	discharge (l/s)	Yield (l/min)	REMARKS
51	Gadaka N11^{0}17'09'' E11^{0}13'11'' Alt. 366m	100	7.1	19.72	0.784	47.06	Moderate Yield
52	Hashidu Primary School N10^{0}53'33'' E10^{0}39'57'' Alt: 332m	45	14.02	0.78	0.794	47.65	Moderate Yield
53	Unguwan Chiroma Lafiya N10^{0}58'32'' E10^{0}41'03'' Alt: 327m	46	16.01	0.85	0.815	48.91	Moderate Yield
54	Wuro Bali N10^{0}44'05'' E10^{0}32'30'' Alt: 334m	45	10.72	3.7	0.758	45.45	Moderate Yield
55	Gafara Galadima N10^{0}36'55'' E11^{0}25'19'' Alt. 281m	39	15	13.46	0.74	44	Moderate Yield
56	Tanglang N9^{0}51'3'' E11^{0}11'5'' Alt. 389m	46	11	12.58	0.8	48	Moderate Yield
57	Federal University Kashere N09^{0}54'54'' E11^{0}00'09'' Alt. 391m	52	13.77	1.95	0.81	48.39	Moderate Yield
58	Gandun Sarki Pindiga N9^{0}59'23'' E10^{0}56'47'' Alt. 511m	60	40.6	0.71	0.81	48.39	Moderate Yield
59	G.J.S.S Tumu N10^{0}00'28'' E11^{0}00'48'' Alt. 414m	45	13.3	3.28	0.77	46.15	Moderate Yield
60	Futuk N09^{0}50'16'' E10^{0}54'01'' Alt. 392m	60	25.66	3.78	0.73	43.69	Moderate Yield
61	Barambu Kolmani N10^{0}7'7'' E10^{0}42'43'' Alt. 318m	75	17	1.89	0.71	42.35	Moderate Yield
62	Kari N11^{0}14'27'' E10^{0}33'13'' Alt. 421m	48	5.5	7.7	0.72	43.2	Moderate Yield
63	Duggal Zange N10^{0}35'22'' E10^{0}46'22'' Alt: 400m	47	22.34	1.09	0.647	38.79	Low Yield
64	PHCC Dukul N10^{0}36'11'' E11^{0}22'35'' Alt. 316m	28	6.8	10.88	0.545	32.73	Low Yield
65	Walama N10^{0}16'57'' E11^{0}57'45'' Alt. 383m	49	28	19.43	0.63	37.5	Low Yield
66	Lamurde N09^{0}36'25'' E11^{0}47'19'' Alt. 177m	75	16	7.2	0.42	25	Low Yield

Appendix (D)

S/NO	location/ coordinates	Borehole depth (m)	Static water Table (m)	draw down (m)	discharge (l/s)	Yield (l/min)	REMARKS
67	Digare N09^{0}39'29" E10^{0}44'60" Alt. 312m	55	14.8	4.52	0.64	38.46	Low Yield
68	Alkaleri N10^{0}16'25'' E10^{0}20'37'' Alt. 384m	75	19.14	24.65	0.64	38.1	Low Yield